Water budget of maize on heavy clay in a continental climate: field experiment and model simulation

Final report of the project "Evaporation estimation comparison"

M. Soet[1], P. Petrovic[2], J.N.M. Stricker[1], W. Meijninger[3], A. van Schaik[3] en T. Lapsansky[2]

1: Department of Water Resources, Wageningen Agricultural University
2: Water Research Institute, Bratislava
3: MSc. students, Wageningen Agricultural University

RAPPORT 67 Juni 1996

Vakgroep Waterhuishouding
Nieuwe Kanaal 11, 6709 PA Wageningen

ISSN 0926-230X

CONTENTS

FOREWORD

The project "Evaporation Estimation Comparison" was carried out in 1995 and 1996 in a joint effort by the Department of Water Resources of the Wageningen Agricultural University (WAU), The Netherlands and the Water Research Institute (WRI) at Bratislava, Slovakia. The contacts between the two groups go back to 1977, when ir. Han Stricker first visited the meteorological station in Ziharec. During the following period contacts were strengthened by mutual visits, including two study stays of dr. Pavel Petrovic at the WAU in 1983 and 1988.

The financial support for the project was provided by the Dutch Ministry of VROM and the Slovakian Ministry of Environment. We would like to thank especially dr. K. Krijt and the Slovak Department of Water Protection for their help and interest. Furthermore, the stay of two Dutch students in Slovakia was partly financed from the EU Tempus program. Also the contribution of the International Agricultural Centre (IAC) by financing a one-month stay of dr. Petrovic in Wageningen and practical arrangements made by Mrs. Van Agen during this period are highly appreciated.

During the field experiment in the summer of 1995 the meteorological station in Ziharec served as home base for maintenance of equipment and primary data analysis. The station staff offered great help in solving practical problems but moreover their enormous hospitality for Dutch students and staff is unforgettable. Also Gijs van den Abeele of the WAU was very helpful with his technical assistance during the preparations and start-up of the experiment. Several Slovakian students took part in the field work, their help in experimental and personal affairs was very constructive.

The results of this project include a comprehensive data set which may be used in future for a number of studies concerning the soil-vegetation-atmosphere system. In principle, this data set is at free disposal for scientific purposes of groups in both Slovakia and The Netherlands.

1. INTRODUCTION

The water budget at the land surface constitutes an important factor in the overall hydrological cycle and as such has a strong impact on the climatic system and agricultural crop production. An improved understanding of the involved meteorological and hydrological processes may therefore lead to more adequate decisions when designing for instance water management projects. Comprehensive field experiments may contribute to this improved understanding and offer the data sets needed to calibrate and validate soil-water-plant-atmosphere models.

In the project "Evaporation estimation comparison", the vertical water budget at the land surface was monitored during the 1995 summer season for a maize crop growing on heavy clay in southern Slovakia. A similar experiment was performed earlier in 1985 on a sandy soil near Renkum, The Netherlands [7, De Boer, 1988]. The different climatic conditions and soil characteristics will offer an interesting possibility to compare experimental and model results. The original intention of the Slovakian experiment was also to study the impact of the Danube Gabcikovo Dam on water regime and crop production in the surrounding area. In this report, however, no special attention is given to this aspect.

The field measurements and data analysis performed within the framework of this project were carried out to meet the following objectives:

- Monitoring of meteorological processes, hydrological processes and crop development of maize during a growing season.
- Calculation of the separate vertical water budget terms, of which evapotranspiration by different methods, and evaluation of results.
- Validation of the conceptual model DAIR by means of the collected data set.
- Validation of the physically based model SWAP93 by means of the collected data set, including the implementation of a recently developed crack module.
- Intercomparison of model results.

To meet the objectives, the setup of the field experiment included measurements of several meteorological parameters like radiation, temperature, wind speed and precipitation, monitoring of soil moisture, ground water level and crop development and additional laboratory measurements to characterize soil physical properties. During the experiment a regular primary data analysis was performed to correct for errors in the experimental setup.

After finishing the field experiment, a thorough analysis of all collected data was performed. A final data set including 30 minute values of evapotranspiration, precipitation, daily ground water level and weekly soil moisture profiles as well as characteristic stages in crop development and soil physical properties resulted. The actual evapotranspiration was calculated by the standard flux profile method and Bowen ratio method. To obtain potential evapotranspiration several methods were applied: Penman, Priestley-Taylor, Makkink, Thom-Oliver and Monteith-Rijtema. The measurements of soil moisture in the upper soil layer were influenced by crack formation during part of the field experiment for which was corrected in the final data set.

The data set was used to validate the models DAIR and SWAP93. The conceptually based DAIR model was developed at the Water Research Institute in Bratislava. Validation results include calculated actual evapotranspiration and ground water level. The model SWAP93 is a physically based, one-dimensional model which yields water budget terms like simulated actual evapotranspiration and surface runoff, soil moisture and pressure head profiles. The main factor in the comparison of model results is therefore the reduction of potential to actual evapotranspiration.

This report documents the field activities, the resulting data set and model validation results. In chapter 2, the setup of the field experiment and primary data analysis as performed during the experiment is described. The theory and data analysis concerning calculation of actual evapotranspiration, potential evapotranspiration and characterization of soil hydraulic properties is given in chapter 3. Also included is a comparison of the water budget terms evapotranspiration and soil moisture depletion.

In chapter 4 the structure of the models DAIR and SWAP93 is described, validation results are presented in chapter 5. Conclusions and recommendations are finally given in chapter 6.

Due to practical limitations, it appeared impossible to perform model runs and analysis in a joint effort by both institutes involved in this project. The DAIR description and simulations were obtained at the WRI in Bratislava (4.2 and 5.1), whereas the SWAP93 simulations were carried out at the Department of Water Resources, WAU (4.3 and 5.2).

2. Field experiment: methods and material

2.1. General description of experimental site

The experimental site was situated near the village Ziharec in the south-eastern part of Slovakia. At this site the water budget components and maize crop development were monitored during the 1995 growing season. The maize crop was planted at April 24 and harvested midst October, the measurements started at June 3 and ended at September 12. The field was selected for its large surface area, hence ensuring a sufficient fetch for the micrometeorological measurements during the entire season (Fig. 2.1).

The site was situated in a typical fluvial landscape with a slight but well visible relief causing wet spots in the lower parts of the field. The soil profile consisted of a loose top layer ($\approx$ 20 cm) with a high organic matter content, still including raw material. Under the top layer a dark heavy clay soil was found with an average depth to 1 meter. This heavy clay layer was underline by a more sandy layer with a colour changing gradually from yellow to light gray and containing manganese fragments.

At the nearby standard meteorological station in Ziharec a number of meteorological parameters, including precipitation and temperature, has been measured during the past 40 years. The average monthly precipitation and air temperature calculated over the period 1954 to 1994 during the growing season and the data obtained at the measurement site in 1995 are presented in Table 2.1. Obviously the months of June and August 1995 were relatively wet, whereas in July the precipitation amount was extremely low with high air temperatures.

The measurement program included monitoring of micrometeorological and hydrological processes, monitoring of crop development and characterization of soil physical properties. The micrometeorological measurements were concentrated at and around two masts and provided the following data: temperature, wind speed, radiation, sunshine duration, soil heat flux, wind direction, precipitation and intercepted rainfall.

The hydrological measurements included monitoring of vertical soil moisture profiles, soil water suction, groundwater level and incidently bare soil evaporation.

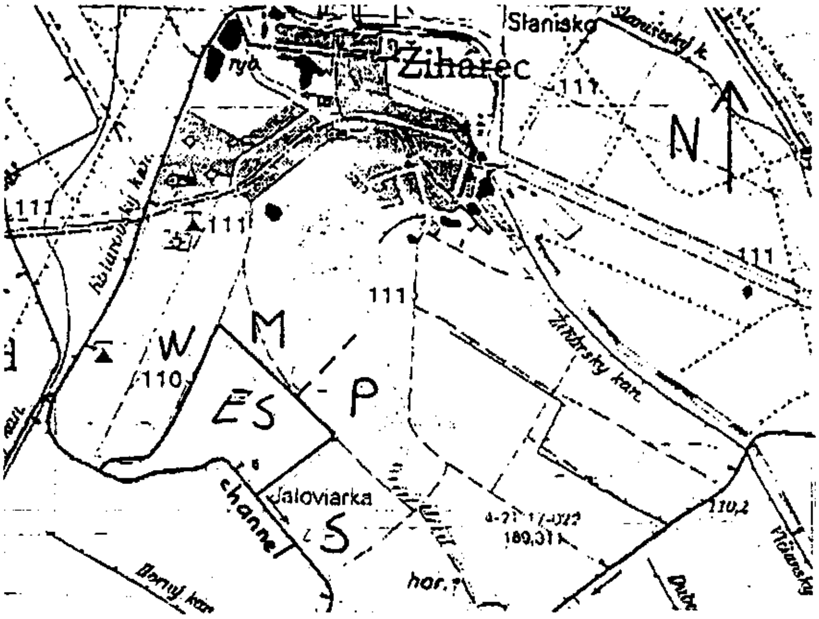

Figure 2.1: Location of the experimental site ES near Ziharec, map 1:50000. Crops at surrounding fields are maize (M), potatoes (P), sunflowers (S) and winter wheat (W)

Crop development was characterized by incidental measurements of crop height, leaf area index, dry matter production, rooting depth and root density profiles. A restricted set of soil physical data was obtained from combined field and laboratory measurements, including clay mineral type, soil water retention data and grain size distribution.

Table 2.1: Monthly precipitation P [mm] and air temperature T_a [°C] average of 1954-1994 and the 1995 growing season

	P 54-94	P 1995	T_a 54-94	T_a 1995
June	66	93	18.4	17.7
July	57	7	19.9	22.8
August	61	80	19.3	19.5
September	38	31	15.3	14.7

2.2. Micrometeorological measurements

2.2.1. Collected data

The micrometeorological monitoring program consisted of measurements of wind speed at two levels, wind direction, net and short-wave incoming and reflected radiation, dry and wet bulb temperature at two levels, sunshine duration, soil heat flux and precipitation, all stored at a temporary resolution of 30 minutes. Fast temperature fluctuations (resolution 1 s) were also measured but not analyzed within the framework of this project. The equipment was installed at or in the vicinity of two height-adjustable masts and connected to a computer and datalogger storing 30 minutes averages or accumulated values. Additionally methods were explored to measure throughfall and "stemflow" after a rainfall event in order to estimate the interception.

The main mast with a maximum height of about 6 meters was equipped with the following instruments at different levels z:

•dry bulb temperature T_{d1} at z_{1h} (temperature sensor)
•dry bulb temperature T_{d2} at z_{2h} (temperature sensor)
•wet bulb temperature T_{w1} at z_{1h} (temperature sensor, natural ventilation)
•wet bulb temperature T_{w2} at z_{2h} (temperature sensor, natural ventilation)
•wind speed u_1 at z_{1m} (cupanemometer)
•wind speed u_2 at z_{2m} (cupanemometer)
•fast temperature fluctuations (1 second) at z_m (thermocouple)
•sunshine duration (Haenni solarimeter).

The wet bulb temperature sensors T_{w1} and T_{w2} could also be used to measure dry bulb temperature. The second, lower mast was equipped with the remaining instruments:

•incoming shortwave radiation $R_{s\downarrow}$ (Kipp radiometer)
•reflected shortwave radiation $R_{s\uparrow}$ (Kipp radiometer)
•net radiation R_n (CSIRO net radiometer)
•wind direction (wind vane).

The soil heat flux was measured with 3 flux plates installed at 5 cm depth in the area covered by the radiation measurements. The soil temperature was measured with a temperature sensor installed partly below the soil surface but through conductance the sensor was assumed to measure surface temperature. Precipitation was measured with a tipping bucket rain gauge (accuracy 0.2 mm) placed at about 10 meters from the main mast and kept 30 cm above crop height. To estimate the interception a regular grid of 40 bottles was installed to determine the average direct throughfall after a rainfall event from the collected water volume in the bottles. Additionally an attempt was made to estimate the amount of rainfall flowing along the stem of plants to the ground. This stemflow was collected in pvc cylinders surrounding the lower stem part of 10 plants.

For a correct analysis of evapotranspiration data the upper and lower measurement of wind speed and temperature at levels z_1 and z_2 need to be taken within the surface boundary layer adjusted to the monitored site (Fig. 2.2). The development of the surface boundary layer over the field depends upon crop height and distance to the field edge leading to the following rules for minimum and maximum sensor heights $z_{\min}$ and $z_{\max}$ [29, Reitsma, 1978]:

$$\begin{aligned} z_{\min} &= 10 * z_0 + d \\ z_{\max} &= f * \mathrm{fetch} + z_0 + d \end{aligned} \tag{2.1}$$

in which z_0 is surface roughness length [m], d zero-plane displacement height [m] and f growth factor of adapted surface layer [$\mathrm{m\,m^{-1}}$]. The factor f is taken to be 1 m growth of boundary layer height per 100 m fetch according to Reitsma [29, 1978], which is a rather safe criterion. The minimum fetch of the selected field for all wind directions was 300 m (see Fig. 2.3). The roughness length for momentum z_{0m} and zero-plane displacement height d were calculated from mean crop height h_c according to [8, De Bruin, 1995]:

$$z_{0m} = 0.11 * h_c \tag{2.2}$$

$$d = 0.67 * h_c \tag{2.3}$$

The height of the main mast with anemometers and temperature sensors was increased regularly during the growing season to fulfill the requirements expressed by (2.1). The lower mast and rain gauge were also adjusted in height, keeping the short-wave and net radiometers at approximately 2 m above the crop surface throughout the growing season.

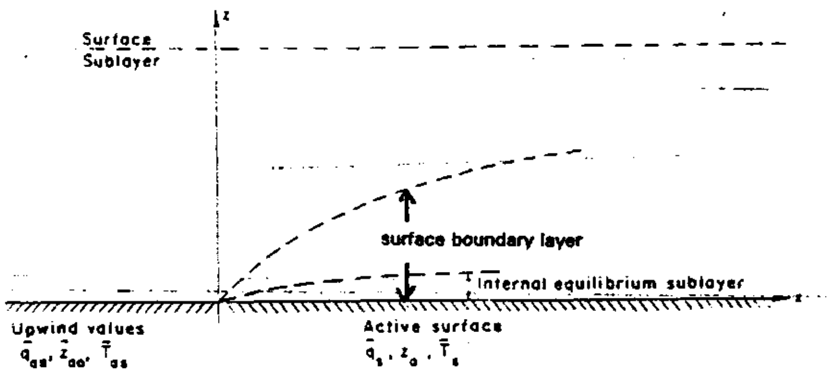

Figure 2.2: Growth of surface boundary layer above a homogeneous surface (source: Brutsaert, 1982)

2.2.2. Data control and correction

The stored data were checked critically during the field campaign hence causes of suspicious results could be quickly detected and corrected if possible. Missing 30 minutes intervals caused by maintenance of instruments were completed in the final data set based upon known data of the same day. Long term missing data due to a computer breakdown were completed using daily averaged data from the standard meteorological station in Ziharec (August 22-28 and September 4).

Dry and wet bulb temperature

The sensors measuring wet bulb temperature in the standard setup were used to measure dry bulb temperature for two 5 day periods, yielding a duplicate measurement of vertical dry bulb temperature difference ΔT_d. The difference of ΔT_d values should be within 0.02 °C to obtain correct evapotranspiration results from calculations with the Bowen ratio method (see 3.2.2). Measured differences exceeded this limit especially around noon at several days (difference of ΔT_d up to 0.08 °C), but no structural cause was detected.

The wet bulb temperatures were sufficiently accurate to calculate the relative humidity r as the ratio of actual water vapour pressure e [mbar] and saturated vapour pressure e_w [mbar] according to [6, Brutsaert, 1982]:

$$r = \frac{e}{e_w(\overline{T_d})} \tag{2.4}$$

The vapour pressure was calculated using the psychrometer equation:

$$e = e_w(\overline{T_d}) - \gamma(\overline{T_d} - \overline{T_w}) \tag{2.5}$$

with γ the psychrometer 'constant' (0.66 mbar °C^{-1}), $\overline{T_d}$ and $\overline{T_w}$ are vertically averaged 30 min values of dry and wet bulb temperature [°C]. The saturated vapour pressure was approximated by [8, De Bruin, 1995]:

$$e_w(T) = e_w(T_0) * 10^{\frac{aT}{b+T}} \tag{2.6}$$

in which $e_w(T_0)$ is the saturated vapour pressure at 0 °C (6.107 mbar), a and b are empirical constants (7.5 and 237.3 °C respectively).

Wind speed and direction

Wind speed measurements might be influenced by the mast itself due to the construction and setup of the main mast with equipment. To prevent this, the mast was turned when necessary in order to adjust the position of the sensors according to the wind direction. Furthermore, structural errors incidentally caused a measured inverse wind profile at wind speeds below 1.5 [$\mathrm{m\,s^{-1}}$] (pers. comm. J.N.M. Stricker). In this range ($u_1 < 1.5$) the wind profile used for the evapotranspiration calculations (see 3.2) was replaced by the measurement of the upper sensor u_2 and a wind speed $u_1 = 0$ at height $d + z_{0m}$.

The roughness length for momentum z_{0m} and displacement height d are calculated from registered crop height h_c according to (2.2) and (2.3). The crop height, however, varied considerably over the field ranging from sections with h_c =120-140 cm to 200-220 cm in August. Hence the values of z_{0m} and d might be related to wind direction, but in the final data set used for further calculations the field average crop height was used to determine z_{0m} and d.

Soil heat flux

The soil heat flux G was measured with 3 flux plates at 5 cm depth. To obtain G at the soil surface the measured value has to be corrected for difference in thermal conductivity λ of the flux plates and the soil and for heat storage in the soil layer above the plates. The correction for thermal conductivity differences was made according to Philip [27, 1961]:

$$\frac{G_{plate}}{G_{corr}} = \frac{\xi}{1 + (\xi - 1)\,H'} \tag{2.7}$$

in which G_{plate} and G_{corr} are measured and corrected soil heat fluxes at 5 cm depth respectively [$\mathrm{W\,m^{-1}}$], H' is a factor depending upon the plate geometry (0.93) and ξ is the ratio of plate and soil thermal conductivity $\lambda_{plate}/\lambda_{soil}$. The soil thermal conductivity λ_{soil} depends upon soil type and soil moisture content θ. Values of λ_{soil} were estimated from literature data [8, De Bruin, 1995] and θ measured by TDR at 5 cm depth.

To obtain the soil heat flux G at the surface, a second correction concerns compensation for heat storage in the upper 5 cm of soil [6, Brutsaert, 1982]:

$$G = G_{corr} + \int_0^z C_s(z)\frac{\Delta T}{\Delta t}\Delta z \tag{2.8}$$

in which T is the estimated soil temperature at 2.5 cm depth [K], t is time [s], C_s is volumetric soil heat capacity [$\mathrm{J\,K^{-1}\,m^{-3}}$] and z is plate depth [m]. The value of C_s at 2.5 cm depth was calculated from the volume fractions of mineral soil θ_m, organic matter θ_c, water θ and air θ_a [6, Brutsaert, 1982]:

$$C_s = C_m\theta_m + C_c\theta_c + C_w\theta + C_a\theta_a \tag{2.9}$$

where the C terms are the volumetric heat capacities [$\mathrm{J\,K^{-1}\,m^{-3}}$] of the different fractions as indicated by the subscripts. The water fraction θ was estimated from

TDR measurements at 5 cm depth, the organic matter fraction θ_c was estimated at 0.10 [$cm^3\,cm^{-3}$] and the mineral fraction was estimated at 0.41 [$cm^3\,cm^{-3}$] by taking the porosity equal to measured saturated moisture content.

The soil temperature at 2.5 cm depth was calculated by assuming that the temperature gradient remained constant over the upper 5 cm soil layer. The temperature gradient at 5 cm depth over a 30 min time interval was obtained from:

$$G_{corr} = -\lambda \frac{\partial T_{5cm}}{\partial z} \tag{2.10}$$

Next the temperature at 2.5 cm depth was calculated from $\partial T/\partial z$ and surface temperature T_s. The measured surface temperature T_s, however, fluctuated too strongly to be representative for the temperature change in the 5 cm soil compartment. Therefore the measured T_s was smoothed using a moving average with a time interval chosen according to:

$$\Delta t = \frac{C_s}{\lambda} (\Delta z)^2 \tag{2.11}$$

where Δt is the characteristic time scale of temperature change for a soil layer with depth Δz ($\Delta t \approx 80$ [min]).

Interception

The throughfall and stemflow volumes were measured immediately after 6 rainfall events throughout the growing season from which the interception I [mm] was calculated via plant density. The interception in most cases amounted approximately 70% of precipitation P which is much higher than values reported in literature, which indicate an average interception of 30% for a maize crop in the growing season [33, Schmidt and Mueller, 1991].

During the field experiment regularly leakage from the experimental stemflow meters was registered which explains the too low measured throughfall + stemflow amounts causing high interception percentages. After each event, however, attempts were made to improve the quality of the construction The last monitored rainfall event at September 4, being the single event for which no leakage was registered at any stemflow meter, yielded an interception of 27%. Hence the explored method might be useful for interception measurements but the construction should be more solid to obtain reliable data. For further data analysis the empirical formula presented by Schmidt and Mueller [33, 1991] was used to calculate the interception I [mm] from precipitation P [mm] and leaf area index LAI [$m^2\,m^{-2}$]:

$$I = -0.521 + 0.528LAI + 0.214P - 0.066LAI^2 - 0.003P^2 + 0.033LAI\,P \tag{2.12}$$

2.3. Soil measurements

2.3.1. General setup

The main part of the soil monitoring program included daily registration of ground water level (3 locations) and measurements of soil water content by Time Domain Reflectometry (TDR) and neutron probe. These measurements were performed on a weekly base but more frequently following a rainfall event: the first, third and sixth day after rain, then again once a week. Neutron probe access tubes were installed at 14 plots to 200 cm depth, except 4 spots where depth was only 140 cm. Since neutron probe measurements close to the soil surface are unreliable, the moisture content of the surface layer was measured by TDR. TDR probes were installed horizontally at 5 and 10 cm depth near 12 neutron probe access tubes. Additionally TDR probes were installed at 40-50 and 100-110 cm depth (vertically) around 3 access tubes which provided data for calibrating the neutron probe measurements.

In combination with vertical TDR probes at 40-50 cm depth tensiometers were installed to measure soil water suction h at 45 cm depth. Tensiometers and TDR were monitored simultaneously hence providing single points of the soil water retention curve $\theta(h)$. Additional tensiometers were installed at 25 cm depth. Since suction measurements with tensiometry become invalid above approximately 850 cm suction, which situation occurred rather early in the field experiment due to severe drought in July, monitoring of tensiometers finished at July 24.

Incidentally, soil evaporation was measured using micro-lysimeters and soil samples for additional laboratory analysis were collected. This included measurement of saturated soil moisture content, grain size distribution and clay mineral type. The general measurement layout and the setup of a plot equipped fully with neutron probe access tube, horizontal and vertical TDR and tensiometers are shown in Figure 2.3 and 2.4.

2.3.2. Calibration of neutron probe and time domain reflectometry

The TDR technique is based on the large dielectric constant value of water (80) compared to air (1) and soil particles (≈ 4), which means that the soil moisture content can be related to bulk soil dielectric constant. The travel time of an electromagnetic signal, transmitted into the soil along a probe and reflected back to the recording instrument at the end of the probe, is measured from which the dielectric constant ε_s can be calculated according to [31, Roth et al., 1990]:

$$\varepsilon_s = \left(\frac{c_0 t}{2L}\right)^2 \tag{2.13}$$

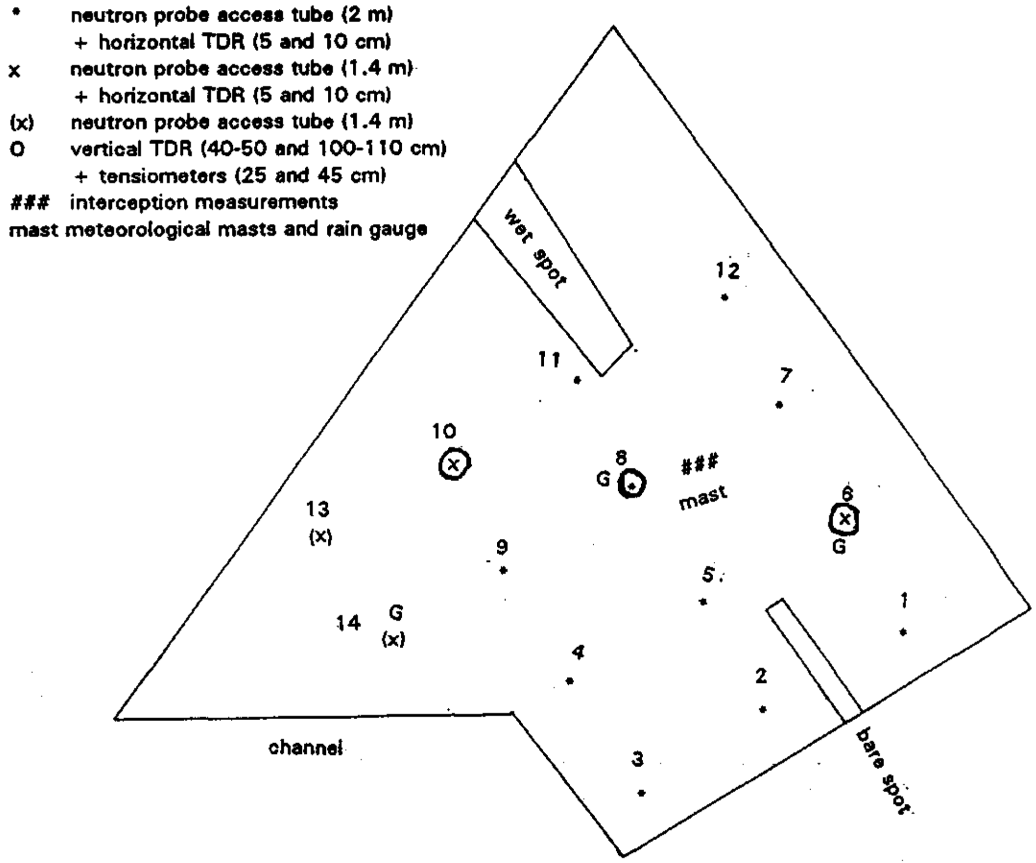

Figure 2.3: Schematic layout of equipment installation at the experimental site ($\approx 1 : 10000$)

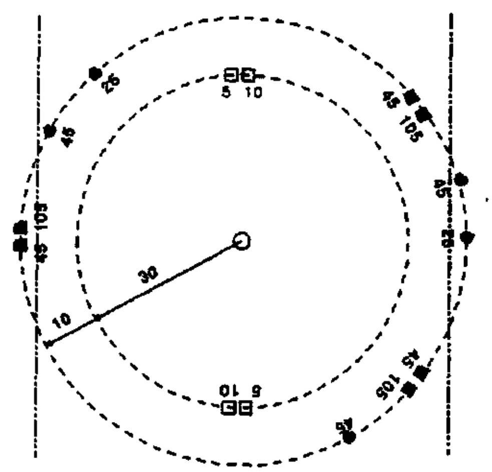

Figure 2.4: Standard layout of fully equipped plot with central the neutron probe access tube, □ is TDR sensor, • is tensiometer (depths in cm) and -.- plant rows

in which c_0 is light speed in vacuum [$\mathrm{m\,s^{-1}}$], t travel time of TDR signal [s] and L probe length [m].

The instrument used was manufactured by Easy Test Ltd, Poland (FOM/m) with a built-in standard $\theta(\varepsilon_s)$ curve. Since the relation between dielectric constant ε_s and soil moisture content θ at heavy clay soils can vary considerably from standard empirical relationships, 22 samples were collected to determine a calibration curve for this specific site. The sample dielectric constant was measured by TDR and the volumetric water content determined by weighing and oven-drying of a known soil volume. Through the measured points a logarithmic curve was fitted with a maximum absolute error of 0.059 % (Fig. 2.5):

$$\theta(\varepsilon_s) = 0.181 \ln(0.596\varepsilon_s + 1.01) - 0.102 \qquad \text{for } \theta \geq 0.10 \tag{2.14}$$

In the range $\theta < 0.15$ [$\mathrm{cm^3\,cm^{-3}}$] no reliable TDR measurements were possible due to crack formation. Equation (2.14) is also assumed to be valid for the more sandy layer starting at about 1 m depth since it was not possible to collect calibration samples in this layer.

TDR measurements were performed at plots 1 to 12 at 5 and 10 cm depth in duplicate (horizontally) and at plots 6, 8 and 10 at depths 40-50 cm and 100-110 cm (vertically) at 3 sides of the neutron probe access tubes (Fig. 2.4). The latter were used for calibration of neutron probe measurements.

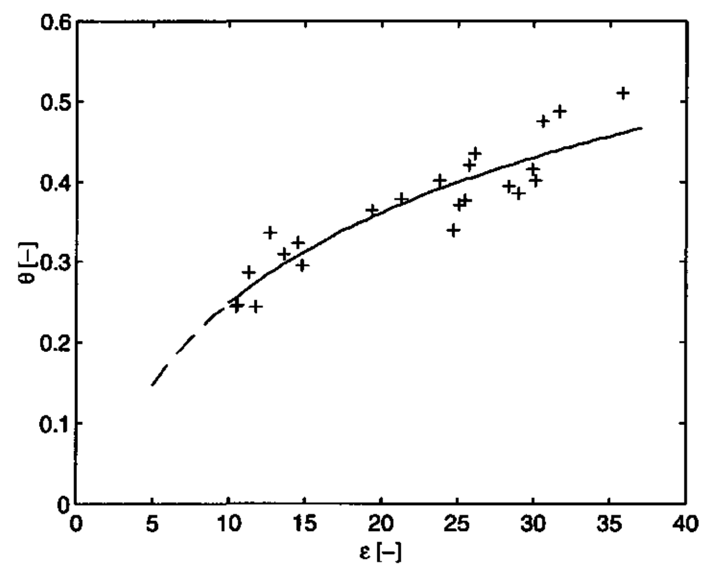

Figure 2.5: Logarithmic TDR calibration curve (solid) fitted through measured points (+)

Fast moving neutrons, emitted into soil from a radioactive source, are predominantly reduced in energy by hydrogen. Therefore, the number of detected low-energy neutrons is related to the moisture content of the surrounding soil volume. In order to calculate the moisture content from count number, the neutron probe has to be calibrated for a particular soil. In general the ratio of measured counts and number of counts in a standard medium is calibrated.

The count ratio was calibrated against TDR measurements according to a method presented by Greacen [12, 1981] which compensates for bias in θ. This correction for sampling errors is obtained from the 3 replicates of measured soil moisture which are available for each single count ratio at 45 and 105 cm depth (3 TDR sensors per depth) and provides a more accurate calibration than classic linear regression. Although the TDR calibration curve (2.14) was only derived for the upper soil layer, a separate curve was fitted for neutron probe data in the layer 0-100 cm and 100-200 cm depth. The resulting calibration curves of count ratio n versus volumetric moisture content θ are given by (Fig. 2.6):

$$\begin{array}{ll} \theta(n) = 0.200n + 0.0166 & \text{layer 0-100 cm} \\ \theta(n) = 0.132n + 0.127 & \text{layer 100-200 cm} \end{array} \tag{2.15}$$

Neutron probe access tubes were installed at 14 plots to a depth of 2 m except for plots 6, 10, 13 and 14 which reached only 1.4 m (Fig. 2.3). Measurements were taken at 20, 30, 45, 65, 85, 105, 120, 140, 160, 180 and 200 cm depth, standard counts were measured twice a week in air. Measurements at 20 and 30 cm became unreliable during dry periods because of soil cracking.

2.3.3. Soil evaporation

Evaporation from bare soil was measured using several pairs of pvc microlysimeters (length 12 and 17 cm, inner diameter 8 cm). These cylinders were carefully pushed into the soil and taken out to seal the bottom of the cylinder in order to prevent water movement between the underlying soil and the sample. After weighing the microlysimeter it was placed back in a preformed hole and taken out every day, weighed and replaced. Evaporation in between measurements was calculated from difference in mass.

The experiment started 3 days after a rainfall event, thereby assuming that downward movement of water would not occur beyond that period. Upward movement of water would also cause a deviation between evaporative loss from the microlysimeter and the surrounding soil. Therefore microlysimeters were installed in pairs of different length assuming that the short lysimeters deviated from true evaporation rate sooner than long ones [3, Boast and Robertson, 1982], hence

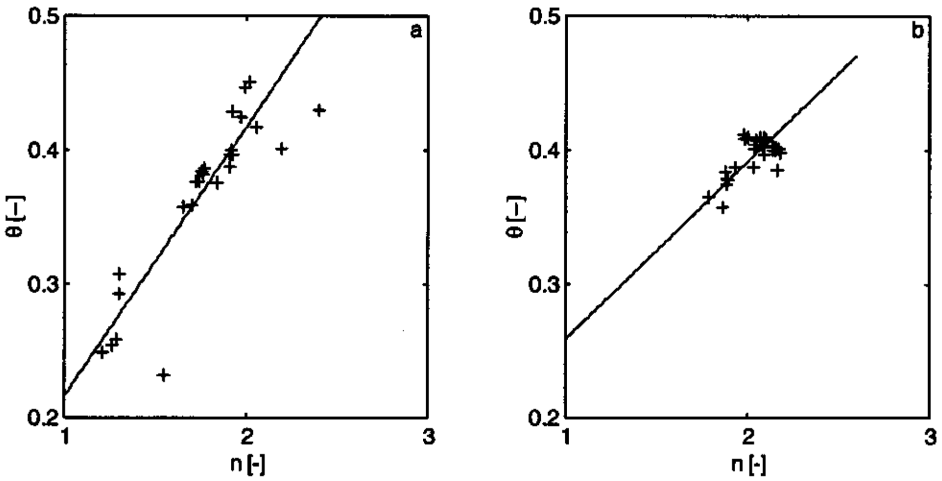

Figure 2.6: Neutron probe calibration curves for 0-100 cm (a) and 100-200 cm (b) fitted through bias corrected soil moisture data (+)

data were reliable when mass loss from both microlysimeters was similar. Finally a 5-day set of evaporation data from 6 microlysimeter pairs was obtained (August 11-15) for a fully developed vegetation.

2.4. Vegetation

Four vegetation parameters were registered: crop height h_c, leaf area index (LAI), dry matter production and root development. Crop height measurements were used to determine the level of wind and temperature sensors and to calculate the roughness length z_0 and zero-plane displacement height d according to (2.2) and (2.3). The time interval for measurements was chosen according to crop development hence measurements were taken less frequent after the crop reached its final height in the beginning of August.

The leaf area index was measured every two weeks till the plants reached maturity. The LAI of a crop sample (minimum 5 plants) was derived by drawing and cutting the leaf contours from paper of known specific weight, weighing the paper and calculating the leaf surface area via the paper surface-weight relationship. Finally LAI was determined using the average field plant density (7.4 plants m^{-2}).

Dry matter production of the LAI samples was measured by weighing the plants immediately after sampling. From the LAI sample a smaller sample was taken and weighed before and after ovendrying at 85 °C during 24 hours. From this the dry matter weight of the original sample was calculated. Since dry matter production was still going on after the plants reached maturity these measurements continued till the end of the field experiment.

During the field experiment an estimate of rooting depth was determined three times by observations in auger holes. The root density profile was determined in the laboratory from samples collected in August near plot 12, which was considered to be representative for the field. The sampling depth was 0-70 cm depth at one location within a plant row and one location in between the rows. After preparing the samples in a salt bath the root length per volume of soil was determined by the root counting technique [18, Koorevaar, 1995].

3. THEORY AND DATA ANALYSIS

3.1. The energy and water budget at the land surface

Evaporation of water is one of the main phases in the hydrological cycle and is the connecting link between the water budget and energy budget at the land surface. The water budget expressing the conservation of mass in a lumped hydrological system over a certain period can be described by [6, Brutsaert, 1982]:

$$(P - ET_{cum})\, A + Q_i - Q_o = \Delta S_w \tag{3.1}$$

in which P is precipitation [cm], ET_{cum} cumulative evapotranspiration [cm], A the surface area [cm^2], Q_i and Q_o are surface and groundwater inflow or outflow respectively [cm^3] and ΔS_w is the change of water storage in the system [cm^3].

The energy needed for evaporation of water is provided by the net radiation R_n reaching the land surface. The net radiation consists of four components:

$$R_n = R_{s\downarrow} - R_{s\uparrow} + R_{l\downarrow} - R_{l\uparrow} \tag{3.2}$$

where $R_{s\downarrow}$ and $R_{s\uparrow}$ [W m^{-2}] are incoming and reflected short-wave radiation respectively and $R_{l\downarrow}$ and $R_{l\uparrow}$ [W m^{-2}] are incoming and outgoing long-wave radiation. The main components of the energy budget equation besides the evapotranspiration or latent heat flux L_vE are the sensible heat flux H and soil heat flux G:

$$R_n = L_vE + H + G \tag{3.3}$$

with all energy fluxes in [W m^{-2}] and L_v the latent heat of vaporization [J kg^{-1}].

In this study the actual evapotranspiration is calculated at 30 minute intervals by the standard flux profile method and Bowen ratio method. Both are energy balance methods in which the components R_n, H and G are determined from measured micrometeorological parameters and L_vE is calculated based upon (3.3) (see 3.2). The actual evapotranspiration can also be calculated on a longer term base from soil water measurements using the water budget equation (3.1), when assuming that the runoff components Q_i and Q_o are negligible. A comparison of results obtained by both approaches is presented in 3.8.

For modelling purposes or prediction of water requirements often the concept of potential evapotranspiration is used. Potential evapotranspiration refers to the maximum rate of evapotranspiration from a large area completely covered by an actively growing vegetation sufficiently supplied by water. Several methods to calculate the daily potential evapotranspiration ET_{pot} were applied: Penman, Priestley-Taylor, Makkink, Monteith-Rijtema and Thom-Oliver (see 3.3). In order to use the methods of Monteith-Rijtema and Thom-Oliver a canopy and aerodynamic resistance have to be specified, which is treated separately in 3.4.

3.2. Actual evapotranspiration

3.2.1. Standard flux profile method

The sensible heat flux H and the momentum flux can be obtained from measured wind and dry bulb temperature profiles using the similarity relations for the surface boundary layer. These similarity relations are based on the Monin and Obukhov [21, 1954] similarity theory, which assumes stationarity and horizontally homogeneous conditions. From dimensional analysis it can be shown that for the description of vertical transport processes in the surface boundary layer the relevant quantities are the height above the surface z, the mean potential temperature θ_T, the air density ρ_a, the gravity acceleration g, the momentum flux or shear stress τ, the sensible heat flux H and the evaporation rate ET_r. Referring to momentum, heat and water vapour transport the following scales can be defined:

$$u_* = \sqrt{\frac{\tau}{\rho_a}} \tag{3.4}$$

$$\theta_* = -\frac{H}{\rho_a c_p u_*} \tag{3.5}$$

$$q_* = -\frac{ET_r}{\rho_a u_*} \tag{3.6}$$

in which u_* [$\mathrm{m\,s^{-1}}$], θ_* [K] and q_* [$\mathrm{g_{water}\,g_{air}^{-1}}$] are the friction velocity or velocity scale, temperature scale and specific humidity scale respectively, c_p is the specific heat at constant pressure [$\mathrm{J\,kg^{-1}\,K^{-1}}$] and ET_r is the evaporation rate [$\mathrm{kg\,m^{-2}\,s^{-1}}$].

With the Monin-Obukhov theory the non-dimensional quantities expressed in (3.4), (3.5) and (3.6), which play a dominant role in the vertical transport of momentum, heat and water vapour in the surface boundary layer, can be written as functions of the dimensionless parameter $\zeta = z/L$ characterizing the atmospheric stability. The Obukhov-length L is defined by:

$$L = \frac{\rho_a c_p T\, u_*^3}{\kappa\, g\, H} \tag{3.7}$$

with L in [m] and κ the Von Karman constant (0.41). By definition $L > 0$ for stable conditions and $L < 0$ for an unstable boundary layer. The set of functions is given by:

$$\frac{\partial \theta_T}{\partial z}\frac{\kappa z}{\theta_*} = \phi_h\left(\frac{z}{L}\right) \tag{3.8}$$

$$\frac{\partial q}{\partial z}\frac{\kappa z}{q_*} = \phi_e\left(\frac{z}{L}\right) \tag{3.9}$$

$$\frac{\partial u}{\partial z}\frac{\kappa z}{u_*} = \phi_m\left(\frac{z}{L}\right) \tag{3.10}$$

The nature of the universal ϕ-functions has been the subject of much theoretical and experimental research and there are still remaining questions concerning the behaviour of these ϕ-functions [6, Brutsaert, 1982], [8, De Bruin, 1995].

For practical purposes it is more convenient to work with the integrated version of equations (3.8), (3.9) and (3.10) [23, Paulson, 1970]. Integrating between the surface and a height z or between two levels above the surface for the temperature and velocity scale yields:

$$\theta_* = \frac{\kappa\left(\theta_{T2} - \theta_{T1}\right)}{\ln\frac{z_{h2}-d_h}{z_{h1}-d_h} - \Psi_h\frac{z_{h2}-d_h}{L} + \Psi_h\frac{z_{h1}-d_h}{L}} \tag{3.11}$$

$$u_* = \frac{\kappa\left(u_2 - u_1\right)}{\ln\frac{z_{m2}-d_m}{z_{m1}-d_m} - \Psi_m\frac{z_{m2}-d_m}{L} + \Psi_m\frac{z_{m1}-d_m}{L}} \tag{3.12}$$

in which z_{x1} and z_{x2} are sensor heights [m] (momentum $x = m$, temperature $x = h$), d_x displacement height [m], θ_{T1} and θ_{T2} potential temperature [K] at level z_{h1} and z_{h2}, u_1 and u_2 wind speed [m s^{-1}] at level z_{m1} and z_{m2} and Ψ_h and Ψ_m are surface layer stability correction terms [-] for momentum and heat respectively.

The surface layer stability corrections (Ψ-functions) under stable conditions ($z/L > 0$) can be expressed by [13, Holtslag, 1987]:

$$\Psi_m = \Psi_h = -A\frac{z_{x,i} - d_x}{L} + B\left(\frac{z_{x,i} - d_x}{L} - \frac{C}{D}\right)\exp\left(-D\frac{z_{x,i} - d_x}{L}\right) + \frac{BC}{D} \tag{3.13}$$

with $A = 0.7$, $B = 0.75$, $C = 5.0$ and $D = 0.35$. For unstable atmospheric conditions ($z/L < 0$) the Ψ-functions are given by [23, Paulson, 1970]:

$$\Psi_h = 2\ln\frac{1+x^2}{2} \tag{3.14}$$

$$\Psi_m = 2\ln\frac{1+x}{2} + \ln\frac{1+x^2}{2} - 2\arctan\left(x\right) + \frac{\pi}{2} \tag{3.15}$$

with $x = \left(1 - 16\frac{z_{x,i}-d_x}{L}\right)^{\frac{1}{4}}$ [-].

From (3.5) it follows that the sensible heat flux H is related to the temperature scale (3.11) and friction velocity (3.12) according to:

$$H = -\rho_a c_p u_* \theta_* \tag{3.16}$$

A similar expression can be derived for the evaporation rate ET_r if humidity profiles are measured in the surface boundary layer. It is more convenient however to calculate the latent heat flux L_vE using the energy budget equation (3.3). In the standard flux profile method, the sensible heat flux H is calculated from (3.11), (3.12) and (3.16) and measured wind speed and dry bulb temperature profiles. Since the net radiation R_n and soil heat flux G are also measured the latent heat flux L_vE can be obtained from (3.3).

3.2.2. Bowen ratio method

This method assumes that the turbulent conductivity or turbulent exchange coefficient K of heat and water vapour are identical [6, Brutsaert, 1982]:

$$K_h = K_v \tag{3.17}$$

In that case the Bowen ratio β, which expresses the ratio between sensible heat flux H and latent heat flux L_vE, can be calculated from temperature and vapour pressure measurements at two levels above the surface:

$$\beta = \frac{H}{L_vE} = \frac{c_p p}{\epsilon L_v}\frac{\Delta T_d}{\Delta e} = \gamma\frac{\Delta T_d}{\Delta e} \tag{3.18}$$

where ΔT_d is the vertical temperature difference [K], ϵ the ratio of molecular weights of water vapour and dry air (0.622), p atmospheric pressure [mbar], Δe the vertical water vapour pressure difference [mbar] and γ the psychrometric "constant" [0.66 mbar K^{-1}]. The value of Δe can be obtained using the vertical wet bulb temperature difference ΔT_w:

$$\Delta e = (s+\gamma)\,\Delta T_w - \gamma\,\Delta T_d \tag{3.19}$$

in which s is the slope of the saturation pressure curve at the vertically averaged temperature $\overline{T_w}$ [mbar K^{-1}].

Combining the energy budget equation (3.3) and the Bowen ratio (3.18) yields the following relations for the sensible and latent heat flux:

$$H = \frac{\beta}{1+\beta}(R_n - G) \tag{3.20}$$

$$L_vE = \frac{1}{1+\beta}(R_n - G) \tag{3.21}$$

The essential principle of the Bowen ratio method is that turbulence is "eliminated" hence no wind speed measurements are needed. The advantage of this method is the proper physical basis, namely the conservation of energy expressed in the energy budget equation. The accurate determination of β, however, is very sensitive to small errors in ΔT_w and ΔT_d. For $\beta = -1$ both (3.20) and (3.21) are undetermined which situation only occurs at the transition from unstable to stable atmospheric conditions (around sunrise and sunset).

3.2.3. Results flux profile and Bowen ratio method

The actual evapotranspiration was calculated from measured data using both the standard flux profile method and Bowen ratio method. Daily (24 h) evapotranspiration results, net radiation, incoming and outgoing short-wave radiation and soil heat flux measured during the field experiment are given in appendix A.

To compare the results of the standard flux profile method and Bowen ratio method the period between sunrise and sunset (800-1800) was taken. Figure 3.1 shows that there is a considerable difference between the resulting latent heat fluxes L_vE. This is especially true for very sunny days (171, 172, 179-182, 202-213, 218, 250). At days 169 and 203 the Bowen ratio β is negative which yields a negative value of L_vE at day 169 and a latent heat flux exceeding the net radiation at day 203. Apparently the Bowen ratio method and flux profile only yield comparable results during partly cloudy, not very sunny periods (day 228-233).

In 2.2.2 the duplicate measurements of dry bulb temperature differences were described. This difference should be within 0.02 °C to obtain sufficiently accurate β-values when measuring both wet and dry bulb temperature profiles. Since these limit was exceeded regularly during the day, for which no structural cause was detected, the results of the Bowen ratio method are considered unreliable. For the model verification presented in chapter 5 the 24 h results obtained by the standard flux profile method are used.

3.3. Potential evapotranspiration methods

3.3.1. Penman method

The equation published by Penman in 1948 [24] was originally intended for evaporation from an open water surface. His formulation is often used, however, to calculate indirectly the potential evapotranspiration for a vegetated land surface. The Penman method has become very popular in hydrological and agricultural practice because only standard meteorological observations are required.

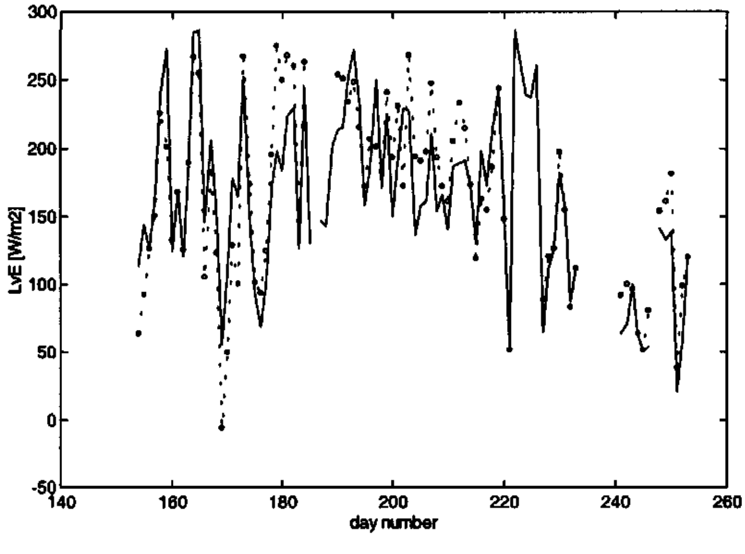

Figure 3.1: Actual evapotranspiration calculated during day time (800-1800) by the flux profile method (solid) and Bowen ratio method (dotted). Daynr 154 = June 3, daynr 254 = Sept 11

The Penman equation is a combination of the energy budget equation (3.3) and the equations of vertical transfer of heat and momentum from a wet surface:

$$H = \rho_a c_p \frac{T_s - T_a}{r_a} \tag{3.22}$$

$$L_v E = \frac{\rho_a c_p}{\gamma} \frac{e_s(T_s) - e_a(T_a)}{r_a} \tag{3.23}$$

where T_s and T_a are surface and air temperature respectively [K], $e_s(T_s)$ saturated vapour pressure at the surface [mbar], $e_a(T_a)$ vapour pressure of the air at T_a [mbar] and r_a is the aerodynamic resistance [$\mathrm{s\,m^{-1}}$]. It is assumed that the aerodynamic resistance r_a is identical for heat and momentum.

In order to solve (3.22) and (3.23) Penman made the following assumption [8, De Bruin, 1995]:

$$e_s(T_s) \approx e_s(T_a) + s(T_s - T_a) \tag{3.24}$$

Substituting (3.24) in (3.23) and combining with the energy budget equation (3.3) now yields:

$$L_v E = \frac{s(R_n - G) + \frac{\rho_a c_p}{r_{a\,\mathrm{penman}}} \Delta e}{s + \gamma} \tag{3.25}$$

in which $r_{a\,\text{penman}}$ is the aerodynamic resistance of a smooth water surface [$\text{s}\,\text{m}^{-1}$] and $\Delta e = e_s(T_a) - e_a(T_a)$ [mbar]. To convert the latent heat flux L_vE [$\text{W}\,\text{m}^{-2}$] to the evapotranspiration rate ET [mm day^{-1}] commonly used in hydrology, one must multiply by a factor $\frac{86400}{2.45*10^6} \approx 0.0352$.

Penman's original equation was based on the empirical wind function structure $f(u)$ introduced by Dalton in 1895 [6, Brutsaert, 1982]:

$$ET = \frac{0.0352\, s\,(R_n - G) + \gamma\, f(u)\; \Delta e}{s + \gamma} \tag{3.26}$$

with the wind function $f(u) = 0.26\,(0.5 + 0.54u_{2m})$ in which u_{2m} is the wind speed at a height of 2 meter. The term $\frac{\gamma f(u)\Delta e}{s+\gamma}$ represents the drying power of the overlying air. The relation between (3.25) and (3.26) is given by:

$$f(u) = \frac{\rho_a c_p}{\gamma\, r_{a\,\text{penman}}} 0.0352 \approx \frac{250}{r_{a\,\text{penman}}} \tag{3.27}$$

The use of (3.26) with the empirical wind function $f(u)$ is adequate to calculate mean values of ET over periods of a day or longer. For shorter term periods the effect of atmospheric stability which is not included may be quite important [6, Brutsaert, 1982].

3.3.2. Monteith-Rijtema method

Originally the Penman equation was derived for evaporation from an open water surface but appeared very useful in practice to estimate indirectly the evapotranspiration from a moist surface completely covered by vegetation. In order to extent this approach, both Rijtema [30, 1965] and Monteith [22, 1965] developed a more general equation which can also be used for a vegetated surface under potential and non-potential conditions. In this formulation a bulk surface resistance parameter r_s was introduced effectively accounting for the stomatal resistance r_l and a resistance depending upon the covered soil fraction r_c:

$$L_vE = \frac{s\,(R_n - G) + \rho_a c_p \frac{\Delta e}{r_a}}{s + \gamma\left(1 + \frac{r_s}{r_a}\right)} \tag{3.28}$$

This Monteith-Rijtema formulation is applicable for all kinds of crops but the bulk resistance r_s and aerodynamic resistance r_a have to be known in order to use (3.28). For potential evapotranspiration conditions for a fully soil covering vegetation normally a bulk minimum resistance value is introduced.

3.3.3. Thom-Oliver method

A certain inconsistency is incorporated in the use of the Penman equation (3.26) for vegetated land surfaces, since the aerodynamic term with the empirical wind function $f(u)$ is derived from land surface data, while the energy balance term is valid for an open water surface. Therefore, Thom and Oliver [35, 1977] generalized the aerodynamic term in Penman's formula while maintaining the use of the empirical wind function.

Thom and Oliver formulated the aerodynamic resistances under neutral conditions r_{an} and non-neutral conditions r_a for any surface as:

$$r_{an} = \frac{\left[\ln\left(\frac{z}{z_0}\right)\right]^2}{\kappa^2 u} \tag{3.29}$$

$$r_a = \frac{\left[\ln\left(\frac{z_\theta}{z_{0h}}\right) - \Psi_h\left(\frac{z_\theta}{L}\right) + \Psi_h\left(\frac{z_{0h}}{L}\right)\right]\left[\ln\left(\frac{z_u}{z_{0m}}\right) - \Psi_m\left(\frac{z_m}{L}\right) + \Psi_m\left(\frac{z_{0m}}{L}\right)\right]}{\kappa^2 u} \tag{3.30}$$

with the Ψ-functions as formulated in 3.2.1. The effect of buoyancy only due to low wind speeds on the aerodynamic resistance is expressed by the ratio $\frac{r_a}{r_{an}}$.

Penman's resistance $r_{a\,\mathrm{penman}}$ introduced in (3.25) is theoretically defined under neutral conditions as:

$$r_{an\,\mathrm{penman}} = \frac{\left[\ln\left(\frac{z}{z_{0p}}\right)\right]^2}{\kappa^2 u} \tag{3.31}$$

in which z_{0p} is the open water surface aerodynamic roughness (1.37 mm). The ratio between r_{an} and $r_{an\,\mathrm{penman}}$ is assumed to be also valid for r_a and $r_{a\,\mathrm{penman}}$:

$$\frac{r_{an}}{r_{an\,\mathrm{penman}}} = \frac{\left[\ln\left(\frac{z}{z_0}\right)\right]^2}{\left[\ln\left(\frac{z}{z_{0p}}\right)\right]^2} = m^{-1} = \frac{r_a}{r_{a\,\mathrm{penman}}} \tag{3.32}$$

With $r_{a\,\mathrm{penman}} = \frac{250}{f(u)}$, as follows from (3.27) and assuming that the roughness length for heat z_{0h} and momentum z_{0m} are identical, r_a can be written as:

$$r_a = m^{-1} r_{a\,\mathrm{penman}} = \frac{\left[\ln\left(\frac{z}{z_0}\right)\right]^2}{\left[\ln\left(\frac{z}{z_{0p}}\right)\right]^2}\frac{250}{f(u)} \tag{3.33}$$

Thom and Oliver included the 'strong' wind function $f(u) = 0.26\,(1 + 0.54u_{2m})$ instead of the 'weak' wind function (3.27) used by Penman [6, Brutsaert, 1982]. Since $\frac{250}{[\ln(z/z_{0p})]^2}$ is 4.72, the aerodynamic resistance is finally expressed by:

$$r_a = 4.72\frac{\left[\ln\left(\frac{z}{z_0}\right)\right]^2}{1 + 0.54u} \tag{3.34}$$

After rearranging the original Penman formulation and including a basic (= minimum) bulk surface resistance similar to the Monteith-Rijtema approach, the Thom-Oliver expression is given by [35, Thom and Oliver, 1977]:

$$ET = \frac{0.0352\, s\,(R_n - G) + m\,\gamma\, E_{ap}}{s + \gamma\left(1 + \frac{r_s}{r_a}\right)} \tag{3.35}$$

in which E_{ap} represents the drying power of the air mentioned in 3.3.1.

3.3.4. Priestley-Taylor method

When air has been in contact with a wet surface over a very long fetch, it may hypothetically tend to become vapour saturated so that the drying power of the air expressed in the Penman formula (3.26) should tend to zero. Hence the radiation term in (3.26) may be considered to represent a lower limit to evaporation from moist surfaces which is called the equilibrium evaporation [6, Brutsaert, 1982].

Priestley and Taylor [28, 1972] have taken equilibrium evaporation as the basis for an empirical relationship giving evaporation from a wet surface under conditions of minimal advection:

$$L_v E = \alpha \frac{s}{s + \gamma}\,(R_n - G) \tag{3.36}$$

with α the Priestley-Taylor coefficient. For large saturated land and 'advection-free' water surfaces Priestley and Taylor concluded that the best estimate for α was 1.26. This value was supported by later studies for well watered grass, potatoes and shallow lakes [6, Brutsaert, 1982]. The $L_v E$ obtained from (3.36) may be considered as a reference value which needs to be multiplied by a certain factor for crops other than grass. However this is no standard practice.

The empirical Priestley-Taylor formulation fails to be valid under circumstances for which the evapotranspiration is mainly determined by large-scale advection and less by radiation. For instance under Dutch conditions, it can only be used from April/May till October.

3.3.5. Makkink method

Makkink's empirical formula relates the potential evapotranspiration of a reference grass crop to the global radiation $R_{s\downarrow}$ [36, TNO, 1988]:

$$L_v ET_{grass} = 0.65 \frac{s}{s + \gamma} R_{s\downarrow} \tag{3.37}$$

The reference grass evapotranspiration ET_{grass} [mm day^{-1}] is officially used by the Royal Dutch Meteorological Institute. To calculate the evapotranspiration for a specific crop, the reference E_{grass} has to be multiplied by a crop factor f_c:

$$E_{crop} = f_c ET_{grass} \tag{3.38}$$

The formulation of Makkink (3.37) is directly related to the Priestley-Taylor equation (3.36) in situations where the global radiation $R_{s\downarrow}$ on a daily base is twice the net radiation R_n [36, TNO, 1988]. The Makkink method is applied during the whole year, however without a clear explanation.

3.4. Determination of resistance parameters

3.4.1. Aerodynamic resistance

The quantity r_a expresses the aerodynamic resistance to the turbulent diffusion of water vapour from the evaporating surface through the air to a reference height. In order to calculate the potential evapotranspiration ET_{pot} with the method of Monteith-Rijtema (3.28) or Thom-Oliver (3.35), the aerodynamic resistance has to be determined. In this study two approaches were applied to calculate the aerodynamic resistance.

The first approach is based upon the formulation of r_a under non-neutral conditions (3.30). Above a high crop, the mechanical turbulence is often much larger than the turbulence produced by buoyancy unless the wind speed is weak. In that case, (3.30) can be simplified by neglecting the stability functions of heat Ψ_h and momentum Ψ_m:

$$r_a = \frac{\ln\left(\frac{z-d}{z_{0m}}\right)\ln\left(\frac{z-d}{z_{0h}}\right)}{\kappa^2 u(z)} \tag{3.39}$$

with $z_{0h} \approx 0.25\, z_{0m}$ [m].

The second approach was developed by Thom and Oliver [35, 1977] as described in 3.3.3. The resulting expression for the aerodynamic resistance r_a is given by equation (3.34). Instead of using different roughness lengths for heat and momentum like in (3.39), it was assumed that $z_{0m} = z_{0h}$ to derive (3.34). Furthermore, the Thom-Oliver method takes implicitly the stability of the atmosphere into account whereas stability effects are neglected in (3.39).

3.4.2. Bulk surface resistance

The bulk resistance r_s expresses the resistance to vapour diffusion from the evaporating surface to the air. For a fully covering crop r_s is mainly composed of the bulk stomatal resistance of the leaves in parallel ('big leaf' approach). When the crop does not fully cover the surface, however, the bulk surface resistance r_s is composed of the stomatal resistance r_l and a resistance r_c depending upon the covered soil fraction and very difficult to determine.

Inversely, the energy balance method [34, Szeicz and Long, 1969] can be used to determine r_s departing from the formulation for potential evapotranspiration from a wet surface ET_{wet}:

$$ET_{wet} = 0.0352 \frac{s\,R_n + \frac{\rho_a c_p}{r_a}\Delta e}{s + \gamma} \tag{3.40}$$

Using (3.28) an (3.35) now as expressions for actual ET (which can be potential) the bulk resistance r_s can be calculated according to:

$$r_s = r_a \left(1 + \frac{s}{\gamma}\right)\left(\frac{ET_{wet}}{ET_{act}} - 1\right) \tag{3.41}$$

The aerodynamic resistance r_a $[\mathrm{s\,m^{-1}}]$ is obtained from equation (3.34) or (3.39) and the actual evapotranspiration ET_{act} is calculated by the standard flux profile method (see 3.2.1).

3.5. Potential evapotranspiration results

The potential evapotranspiration calculated by the methods of Penman, Priestley-Taylor and Makkink (no crop factors included) is shown in Figure 3.2. It can be seen that the Priestley-Taylor method yields slightly higher values than the Makkink method during the growing season. This is caused by the fact that the ratio of net radiation R_n and global radiation $R_{s\downarrow}$ is not identical for a grass covered surface $\left(\frac{0.65}{1.26} \approx 0.52\right)$ and a maize crop $\left(\frac{R_n}{R_{s\downarrow}} \approx 0.58\right)$. At some days the Penman formulation yields relatively high ET_{pot}-values. This is due to a strong wind on those days, causing a significant effect of the advection term which is ignored in the methods of Priestley-Taylor and Makkink.

The aerodynamic resistance r_a was calculated by (3.39) for the Monteith-Rijtema method and (3.34) for the Thom-Oliver method, in both cases for the period between 800-1800 hours.. Results are shown in Figure 3.3. During the growing season r_a for both methods shows a general decrease when the crop height h_c increases. Comparing the two equations, it appears that the discrepancies in the results of r_a can mainly be attributed to the difference of expressions in the denominator. Therefore, (3.34) should be given more credit than (3.39) because it accounts for buoyancy effects at low wind speed.

Since most of the evapotranspiration takes place during daytime, data averaged from 800-1800 were used to calculate values of ET_{wet} in (3.40) and r_s in (3.41). The resulting values of the bulk resistance r_s are shown in Figure 3.4. During the

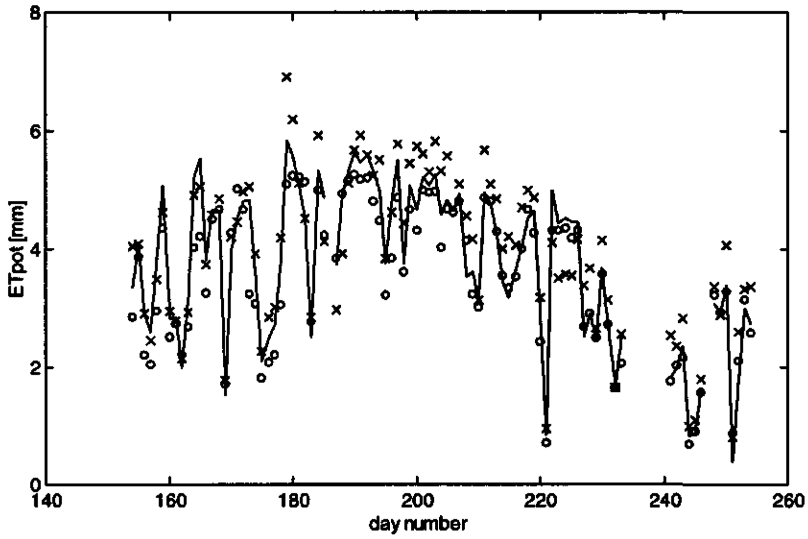

Figure 3.2: Potential evapotranspiration calculated by the methods of Penman (xx), Makkink (oo) and Priestley-Taylor (solid)

dry periods in the growing season, when the water supply in the soil lags behind the evaporation demand, the leaf-water potential decreases hence r_s increases. Similarly it can be seen that r_s decreases after a rainy day or wet period.

In Figure 3.5 the course of bulk and aerodynamic resistance during one day (day number 184) is shown. For this case all the expressions have been applied for 30 min intervals. During most of the day r_s remains more or less constant with a gradual increase in the late afternoon. This suggests that the water supply mainly keeps pace with the evaporation demand. The aerodynamic resistance remains constant during the day with an increase in the early morning and late afternoon when the wind speed decreases. This agrees with results obtained by Jacobs [14, 1989] who found a similar pattern for a maize crop in The Netherlands.

When applying the Monteith-Rijtema and Thom-Oliver method, however, a remaining question is whether the calculated ET in this study will represent a 'true' value of potential evapotranspiration due to problems encountered in determining the resistance parameters. The first point is, whether data averaged between 800-1800 are representative for a whole day. Secondly, the actual evapotranspiration is used in (3.41) to calculate r_s. Due to these problems, the minimum bulk stomatal resistance throughout the growing season cannot be specified adequatly. Therefore, the evapotranspiration calculated by both the methods of

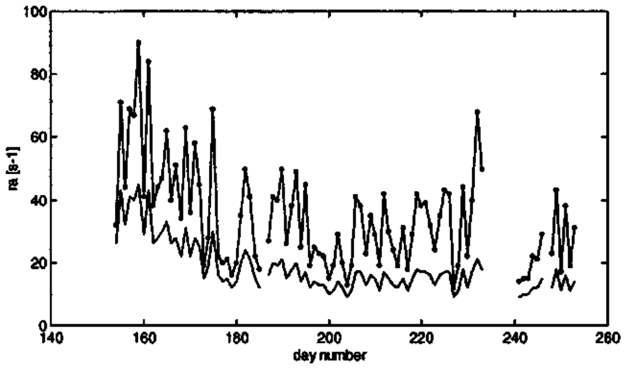

Figure 3.3: The aerodynamic resistance of maize calculated by equation (3.34) (solid) and (3.39) (∘∘)

Monteith-Rijtema and Thom-Oliver is not considered to be a true potential value and ET_{pot}-results are not presented here.

Daily values of potential evapotranspiration ET_{pot} calculated by the methods of Priestley-Taylor, Penman and Makkink are given in Appendix B.

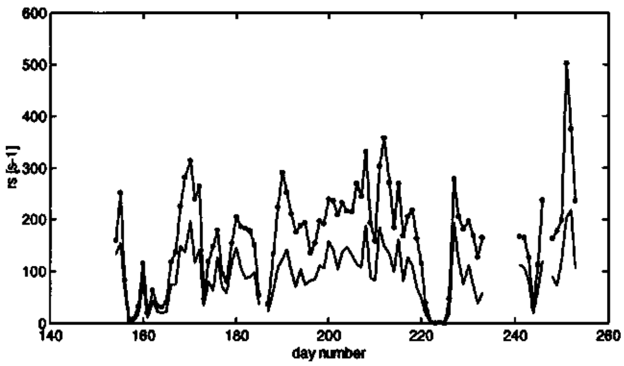

Figure 3.4: The bulk surface resistance of maize calculated by the energy balance method using r_a obtained by (3.34) (solid) or (3.39) (∘∘)

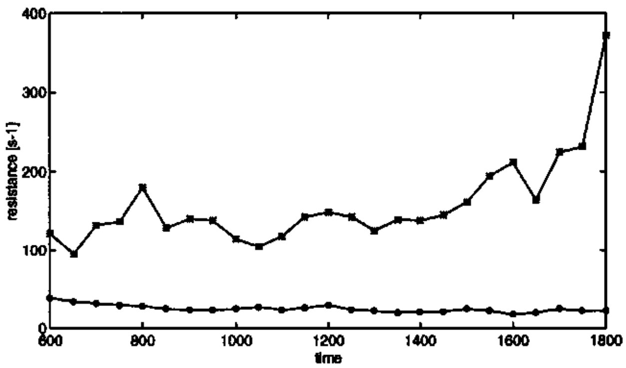

Figure 3.5: The daily course of the aerodynamic (oo) and bulk resistance (**) on day number 184

3.6. Soil related measurements

3.6.1. Ground water level

The ground water level was measured daily at 3 locations (Fig. 2.3). The course of the average ground water level during the field experiment and the precipitation amounts are shown in Figure 3.6. During the first part of the field experiment the ground water level was quite shallow (-30 to -65 cm) due to a wet period in June. Next, the level gradually decreased to -120 cm during a very dry period in July and August. From day number 220 till the end of the field experiment the ground water level only varied between -110 and -130 cm due to regular rainfall during this period.

3.6.2. Soil properties

Hydraulic characteristics

The soil water retention and hydraulic conductivity curves $\theta(h)$ and $k(h)$ can be described analytically according to [37, Van Genuchten, 1980]:

$$\theta(h) = \theta_r + \frac{\theta_s - \theta_r}{(1 + |a_g h|^n)^m} \tag{3.42}$$

$$k(h) = k_s \frac{\left([1 + |a_g h|^n]^m - |a_g h|^{n-1}\right)^2}{(1 + |a_g h|^n)^{ml}} \tag{3.43}$$

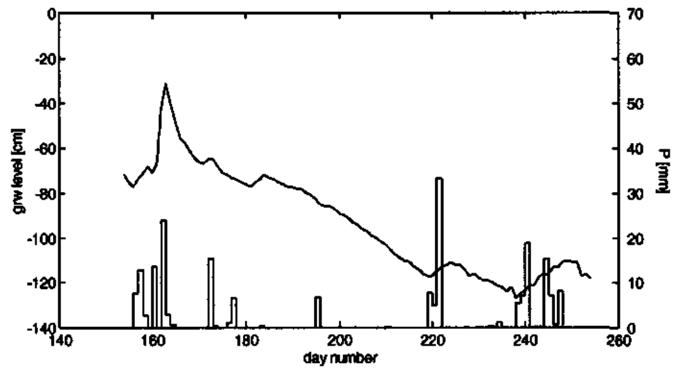

Figure 3.6: Measured daily ground water level and precipitation during the growing season

Table 3.1: Parameters characterizing the soil water retention and hydraulic conductivity curve

a_g [cm^{-1}]	n [-]	θ_s [$\mathrm{cm}^3\,\mathrm{cm}^{-3}$]	θ_r [$\mathrm{cm}^3\,\mathrm{cm}^{-3}$]	k_s [$\mathrm{cm\,d}^{-1}$]	l [-]
0.0532	1.081	0.489	0	15.46	-8.823

in which θ is the volumetric moisture content [$\mathrm{cm}^3\,\mathrm{cm}^{-3}$], θ_s and θ_r saturated and residual moisture content respectively [$\mathrm{cm}^3\,\mathrm{cm}^{-3}$], h soil matric head [cm], k hydraulic conductivity [$\mathrm{cm\,d}^{-1}$], k_s saturated hydraulic conductivity [$\mathrm{cm\,d}^{-1}$] and a_g [cm^{-1}], n and l [-] are empirical parameters with $m = 1 - \frac{1}{n}$.

During the field experiment combined measurements of θ by TDR and h by tensiometry were made at 3 plots (Fig. 2.3). The saturated moisture content θ_s of 20 undisturbed 100 cm^3 samples was determined in the laboratory yielding a field average value of 0.489 [$\mathrm{cm}^3\,\mathrm{cm}^{-3}$]. The resulting set of $\theta(h)$ data, however, provided insufficient information over the entire moisture content range to fit the empirical parameters in (3.42). Therefore, values found in literature [39, Wösten et al., 1994] for clay soils were used to describe $\theta(h)$ and $k(h)$ (Table 3.1). By adjusting only for θ_s, the chosen retention curve fitted well (visually) through the measured $\theta(h)$ data from the experimental site.

Grain size distribution

During installation of the ground water and neutron probe access tubes, disturbed samples were collected to a depth of 200 cm. The grain size distribution of some samples was analyzed according to the standard procedure used by the BGG ("Bedrijfslaboratorium voor Grond- en Gewasonderzoek", Oosterbeek, The Netherlands). This procedure includes sieving of mineral fractions $> 50\,\mu m$ whereas fractions $< 50\,\mu m$ are separated by a technique based upon differences in sedimentation speed for particles of different size.

In total 4 samples were analyzed, being mixed samples of different locations from depth $30-40$ cm, $70-90$ cm, $130-150$ cm and $190-200$ cm. The resulting mass fractions are given in Table 3.2. Obviously the clay and silt percentage (fraction $< 2\,\mu m$ and 2-50 μm respectively) gradually decrease with depth while the percentage sand (50-2000 μm) increases. The textural soil class of the layers according to Table 3.2 changes from clay to sandy clay loam, sandy loam and finally loamy sand [19, Koorevaar et al., 1983].

Table 3.2: Average grain size distribution at experimental site

fraction [μm]	30-40 cm	70-90 cm	130-150 cm	190-200 cm
0-2	54.3	30.8	13.3	7.0
2-16	17.2	10.2	8.0	4.0
16-50	11.3	10.7	7.2	8.3
50-105	4.0	8.2	13.3	15.9
105-150	3.8	10.5	16.0	16.4
150-210	4.5	13.5	23.3	23.5
210-300	3.5	117	13.8	20.2
300-2000	1.4	4.4	5.1	4.7

Shrinking characteristic

The behaviour of a clay soil with respect to swelling and shrinkage during wetting and drying, described by the shrinking characteristic, strongly depends upon the clay mineral types found in a specific soil. The clay type found at the experimental site in the upper layer to ≈ 60 cm depth was determined qualitatively in the laboratory by X-ray analysis and consisted mainly of montmorillonite (at least 50%) with smaller percentages of kaolinite and illite. The shrinking characteristic was chosen according to results presented in literature for a similar soil, namely heavy river clay from Bruchem, The Netherlands [5, Bronswijk, 1991].

In the general shrinkage characteristic four shrinkage stages are distinguished: structural, normal, residual and zero phase. The shrinkage characteristic shown in Figure 3.7 is described by [15, Kim, 1992]:

$$e(\nu) = \alpha \exp(\beta\nu) + \gamma\nu \tag{3.44}$$

in which e and ν are void ratio and moisture ratio respectively, described by $e = \frac{V_p}{V_s}$ and $\nu = \frac{V_w}{V_s}$ where V_p, V_s and V_w are total pore volume, solid volume and water volume [cm^{-3}] respectively. The parameters α, β and γ describe the shrinkage characteristic in the residual shrinkage phase. Values of the dimensionless fitting parameters e_0, ν_1 and ν_s, which determine the transition between the different shrinkage stages, are given in Table 3.3 for the Bruchem river clay. Additional parameters which are needed for model validation are the depth S_c at which the crack area A_c for surface infiltration is calculated, a geometry factor R_s, a rate coefficient for bypass flow to drains or ditches k_d and a polygon diameter D (see 4.3.5)

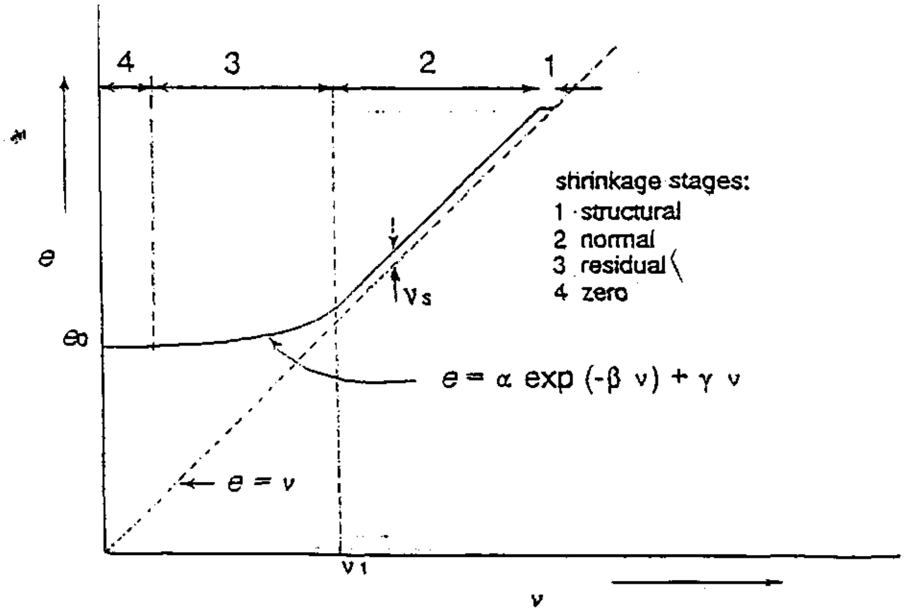

Figure 3.7: The general shrinking charactertistic with the parameters e_0, ν_1 and ν_s

Table 3.3: Dimensionless fitting parameters and model parameters describing the shrinking characteristic of the Bruchem heavy river clay

e_0 [-]	ν_1 [-]	ν_s [-]	S_c [cm]	R_s [-]	D [cm]	k_d [s^{-1}]
0.4	0.5	0	-5.0	3.0	40.0	0

3.6.3. Soil evaporation

Measurements of soil evaporation resulted in a data set of evaporation from 6 microlysimeter pairs for the period of August 11 to 15 and fully grown maize. The cumulative evaporation during this period is plotted in Figure 3.8. From this data set the constants used in two different models to calculate soil evaporation can be calculated.

The Black model [2, Black et al., 1969] was one of the earliest parametric models to estimate the bare soil evaporation. The model describes the cumulative actual evaporation as:

$$\sum E_{act} = \alpha_B t^{\frac{1}{2}} \tag{3.45}$$

in which α_B is a parameter characterizing the evaporation process [$\mathrm{mm\,d^{-0.5}}$] and t is time after preceding rainfall [d]. Black obtained an α_B value of 5 $\mathrm{mm\,d^{-0.5}}$. Klaghofer [16, 1974] obtained a value of 7 $\mathrm{mm\,d^{-0.5}}$. From the experimental data over the period August 11 to 15, a value of 4.7 $\mathrm{mm\,d^{-0.5}}$ is obtained.

The disadvantage of the Black model is that the value of α_B depends implicitly upon the potential evaporation E_{pot} which may vary for instance between 1 and 6 $\mathrm{mm\,d^{-1}}$ in The Netherlands. Therefore, Boesten and Stroosnijder [4, 1986] developed a new model in which the constant β does not depend on E_{pot}. This parametric model is described by:

$$\begin{aligned} \textstyle\sum E_{act} &= \textstyle\sum E_{pot} && \text{for } \textstyle\sum E_{pot} \leq \beta^2 \\ \textstyle\sum E_{act} &= \beta\,(\textstyle\sum E_{pot})^{\frac{1}{2}} && \text{for } \textstyle\sum E_{pot} > \beta^2 \end{aligned} \tag{3.46}$$

in which β [$\mathrm{mm^{0.5}}$] is an evaporative soil parameter determined experimentally. Boesten and Stroosnijder [4, 1986] found a value of 1.7 $\mathrm{mm^{0.5}}$. From the data of our experimental site a value of 1.9 $\mathrm{mm^{0.5}}$ was obtained.

3.7. Crop development

The field average crop height h_c was difficult to determine because the variation over the field was quite large, varying from 1.5 to 2.5 m by the end of the growing season. The finally estimated average value, used to determine the roughness length z_0 and displacement height d according to (2.2) and (2.3), is shown in Figure 3.9. Also presented in Figure 3.9 is the leaf area index LAI which reached its maximum in the middle of August.

The increase of rooting depth during the growing season was difficult to determine due to practical problems with the hard dry soil in July. However, at three days an estimate of rooting depth was obtained yielding a rooting depth of 20 cm at June 15, 50 cm at June 23 and 110 cm at August 15. The course of

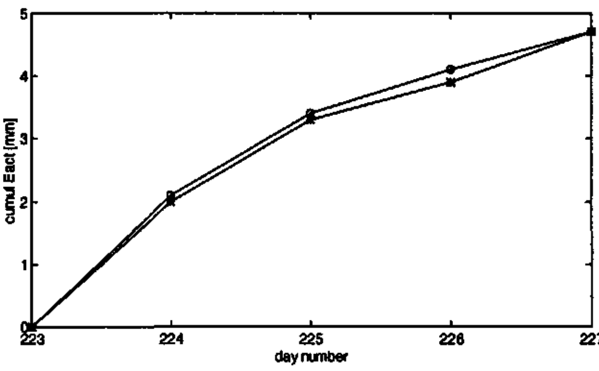

Figure 3.8: Cumulative evaporation from August 11 to 15 after 45.9 mm of rainfall during the period August 7 to 9

the rooting depth over the growing season was estimated by linear interpolation between these data. Since the maximum ground water level was only 130 cm below the soil surface, it is assumed that the crop did not suffer any severe water shortage during the field experiment.

The root density profile was determined in the laboratory from samples taken in August over 0-84 cm depth. One sampling profile was taken between plants within a row and a second profile in between rows. The number of roots found in the first profile was significantly higher than in the second, in both cases the vertical root density distribution was rather irregular. For modelling purposes it was assumed that roots are distributed vertically uniform over the soil profile.

3.8. Water budget comparison

The vertical soil moisture profiles can be used to calculate the change of water storage in the soil profile. According to (3.1) this soil moisture depletion ΔS_w may be compared with actual evapotranspiration ET_{act} over a drying period when assuming that the inflow Q_i and outflow Q_o to the field are negligible. Results for several periods with no precipitation are given in Table 3.4. The field average value of ΔS_w was calculated over the zone from the soil surface to about 20 cm below measured ground water level in order to eliminate the effect of fluctuations in neutron probe measurements.

Apparently the soil moisture depletion over short term periods yields values which are generally lower than ET_{act} over the same period. However, the determination of ΔS_w over these short periods is not considered very accurate. Changes

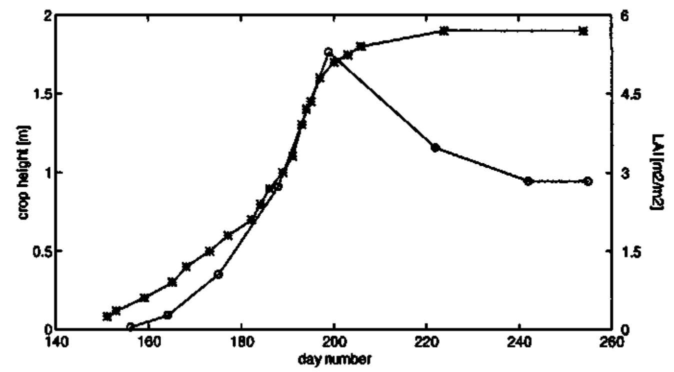

Figure 3.9: Average crop height ($*$) and leaf area index ($\circ$) during the growing season

of soil moisture content θ in the top soil layer (0-30 cm) contribute for a great deal to ΔS_w while measurements in this layer are not very reliable due to crack formation. Over the entire experimental period, however, the profile from 0 to about 140 cm depth contributes to the changes in soil moisture content and the separate water budget terms should be comparable. Considering this period, the difference between ΔS_w and cumulative ET_{act} yields 219 mm which is indeed very close to the total amount of precipitation ($P = 206$ mm).

Table 3.4: Comparison of actual evapotranspiration and soil moisture depletion during drying periods and over the entire growing season

period	ΔS_w [mm]	ET_{act} [mm]	$ET_{act} - \Delta S_w$ [mm]
June 14 - 17	3.8	11.3	7.5
June 17 - 20	2.2	5.4	3.2
June 28 - 30	3.1	6.9	3.8
June 30 - July 4	6.4	12.9	6.5
July 4 - 10	18.1	13.3	−4.8
July 17 - 24	18.8	22.6	3.8
July 24 - Aug 7	23.7	37.4	13.7
Aug 14 - 18	2.3	9.7	7.4
June 3 - Sept 8	56	275	219

4. Model description

4.1. Introduction

Models are valuable tools to study and predict terms of the vertical water budget. Simulation of transpiration and crop production in an agricultural system indicates for instance whether supplemental irrigation is justified under specified conditions. Both models tested within this project are one-dimensional models developped to study processes in the ground water-soil-vegetation-atmosphere system.

The model DAIR (**DA**ily **IR**rigation) was originally developed in 1981 by the Department of Mathematical Modelling in Hydrology, WRI, Bratislava. Part of the model subroutines were improved in 1983 during a study stay at the Wageningen Agricultural University [25, Petrovic, 1984]. Within the framework of the Danubian lowland study in the Gabcikovo dam area, an adjusted version of the model called DINUND (Danube **INUND**ation) was developed to include also floodplain vegetation and hydrological conditions.

The model SWAP93 (**S**oil **W**ater **A**tmosphere **P**lant, version 1993) is an improved version of the physically based model SWATRE [11, Feddes et al., 1978]; [1, Belmans et al., 1983]. The main changes relevant to this study are an improvement of the discretization and solution scheme of the Richards' equation, adjusted top boundary conditions during infiltration and implementation of the Van Genuchten parameters to calculate the soil hydraulic functions [38, Work group SWAP, 1994]. Recently a crack module was added to the model which calculates the effect of swelling and shrinkage in clay soils on the water budget terms.

DAIR is a conceptual, quasi steady state model operating internally with a one day time-step. SWAP is a physically based model, hence it contains fewer assumptions regarding the physics of unsaturated flow. Therefore the internal time-steps are much smaller, depending upon changes in the system. Both models use daily potential evapotranspiration as input at the upper boundary condition. At the bottom boundary SWAP needs input like daily ground water level or pressured head values, in DAIR the ground water level at the bottom boundary is the result of computed fluxes and water balance.

4.2. Model DAIR

4.2.1. Composition of the model

The input data of DAIR consist of three groups:

- formal parameters
- parameters describing soil-physical properties, irrigation regime and vegetation cover development (with a possibility to choose crop rotation for 4 to 8 agricultural plant types)
- daily meteorological input data (precipitation, air temperature and humidity).

Based upon the daily meteorological input the model calculates the potential evapotranspiration ET_{pot}, the actual evapotranspiration ET_{act}, total soil moisture in the selected soil layer SM, seepage as a contribution to the ground water reservoir Q_{seep}, the ground water level h_{gw}, capillary rise from ground water level to the unsaturated soil profile Q_{cap} and contribution of the model areal unit to the runoff from the area Q_o as a function of ground water level. The evaluation of all calculated data is running simultaneously for a natural moisture regime of the area and for a regime with supplementary irrigation.

The present version of the model can work all year round for a maximum of 50 years. Formal limitations force the model to start at January 1, computations can stop at any time. Since in this study only data collected during the growing season is available for model validation, the model description is limited to parts relevant for this period. A brief model description was given previously in several publications [25, Petrovic, 1984]; [26, Petrovic, 1989]; [17, Koopmans, 1990].

4.2.2. Upper boundary condition

At the upper boundary the potential evapotranspiration is calculated according to Budyko's method. After a long term study this method was simplified to a set of nomograms for different geo-botanical zones by the Russian State Hydrological Institute [32, 1976]. The nomograms yield monthly values of potential evapotranspiration for individual or in some cases combined months. Based upon the mean climatic characteristics, the nomogram for a forest-steppe is most suitable for the Slovakian lowlands in which the field experiment was situated (Fig. 4.1). The monthly ET_{pot}-values obtained from this nomogram by digitalization were divided by the number of days in each month, yielding daily values of ET_{pot} as a function of vapour pressure deficit VPD in tabular form.

To eliminate non-homogeneous jumps caused by crossing the boundary between two months or two given values of VPD, the model uses planar interpolation. By assuming that the curve of ET_{pot} versus VPD is valid exactly in the middle of a specific month the interpolation between neighbouring months according to the date is processed. A similar interpolation is done to obtain the exact value of VPD at a specific day. This procedure allows to estimate the value of ET_{pot} for every day individually. The resulting values which are used in the model are given in Appendix C.

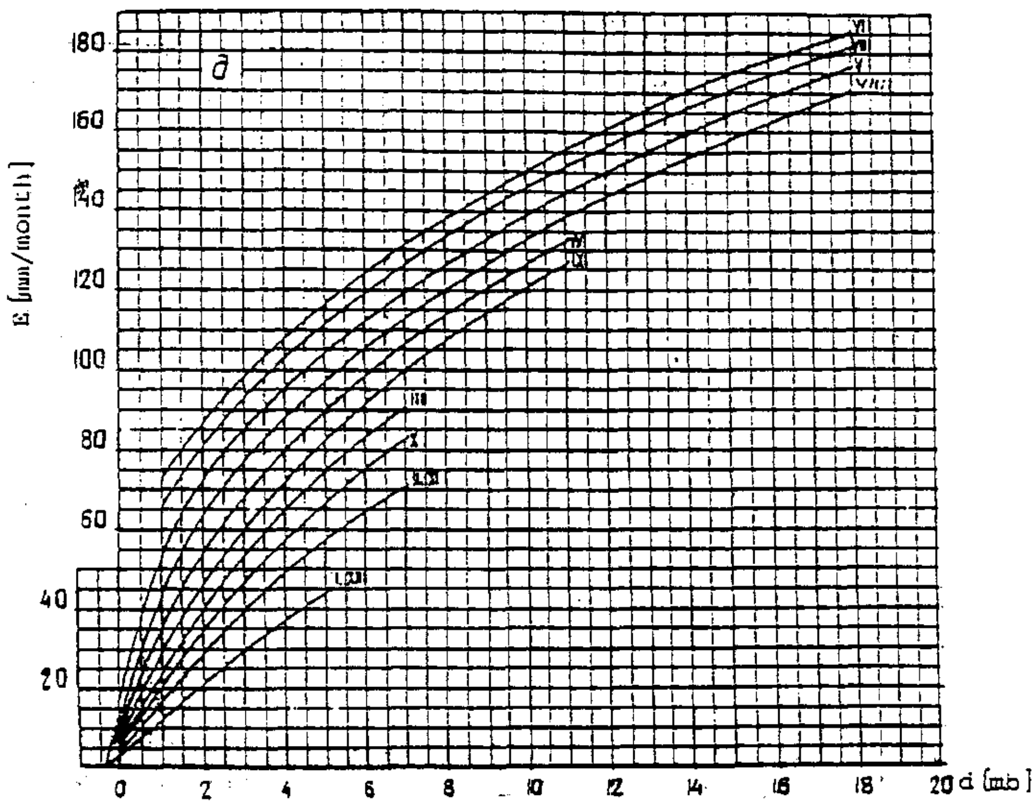

Figure 4.1: Monthly potential evapotranspiration as a function of saturation deficit according to Budyko's method for a forest steppe

4.2.3. Soil moisture, seepage and capillary rise

In DAIR, the total precipitation amount is supposed to infiltrate into the modelled soil column with depth D. Interception is neglected by assuming that all intercepted rainfall evaporates but uses practically the same energy like water transpirated by the crop, hence the total amount of evapotranspiration is not influenced by interception.

The hydraulic characteristics needed are the retention and hydraulic conductivity curves $\theta(h)$ and $k(h)$. From these characteristics the values of porosity ϕ, field capacity SM_{fc}, wilting point SM_{wp} and available soil moisture SM_{av} are determined. The soil moisture SM is considered to be the total amount of water stored in the simulated soil column. After a rainfall event, the value of SM is increased by the amount of infiltrating precipitation. In case that the calculated value of SM exceeds the field capacity, all surplus water is considered to be seepage contributing to the ground water reservoir.

Capillary rise is included in DAIR for ground water levels less than 2 m below the reference level (which is usually the root zone depth) and soil moisture values less than SM_{fc}. Since usually only a limited range of ground water levels and SM-values are simulated, it is assumed that the saturated capillary rise Q_{cap1} [$\mathrm{mm\,d^{-1}}$] can be calculated according to:

$$Q_{cap1} = \begin{array}{ll} DEF + ET_{act} & \text{for roots in saturated zone} \\ \exp(gflco1 - gflco2 \log(DGR)) & \\ 0 & \text{for } DGR > 2 \text{ m or } Q_{cap1} < 0.001 \end{array} \tag{4.1}$$

in which DGR is depth of ground water level below the root zone and values of $gflco1$ and $gflco2$ can be evaluated by the least squares method from laboratory data of upward flow of water for a specific soil layer or by special processing of the $\theta(h)$ curve for the expected range of ground water levels.

Analysis of the matrix of capillary rise for Ziharec obtained by solving the upward flux depending upon the soil moisture content and depth of ground water level showed that the combined drafting force and soil drying processes can be simplified as:

$$DEF = SM_{fc} - SM \tag{4.2}$$

$$RDEF = \begin{array}{ll} 1 & \text{for } DEF \geq 0.4SM_{av} \\ 2.5\frac{DEF}{SM_{av}} & \text{for } DEF < 0.4SM_{av} \end{array} \tag{4.3}$$

$$Q_{cap2} = \begin{array}{ll} Q_{cap1} & \text{for roots in saturated zone} \\ Q_{cap1}\,RDEF & \text{for } DGR > 0 \end{array} \tag{4.4}$$

4.2.4. Actual evapotranspiration

The evaluation of the actual evapotranspiration for the simulated crop consists of two steps. The first step concerns the calculation of crop potential evapotranspiration, in the second step the actual evapotranspiration is calculated depending upon crop potential evapotranspiration and actual soil moisture.

According to the FAO [9, Doorenbos and Pruitt, 1977]the potential evapotranspiration obtained by the method described in 5.1 can be considered as the comparable evapotranspiration ET_o. The potential evapotranspiration for a specific crop can be calculated according to:

$$ET_{crop} = k_c ET_o \tag{4.5}$$

in which k_c is a crop factor. Values of k_c are given for nearly 40 crop types by Doorenbos and Pruitt [9, 1977].

The use of a simple calendar based relationship between the actual day in a growing season and stage of the plant development does not account for the yearly meteorological variability, especially in long time series processing. To eliminate the effects of such a variability, which is significantly dependent upon the meteorological history in a specific growing season, the sum of positive daily air temperatures was introduced as a parameter quantifying the crop development process. This parameter is used to obtain the actual value of the crop factor k_c, root zone depth d_r and for irrigation purposes a lower limit of critical soil moisture.

The actual evapotranspiration depends on the soil moisture SM according to:

$$ET_{act} = f\left(ET_{crop}, SM\right) = ET_{crop} f\left(SM\right) \tag{4.6}$$

in which $f\left(SM\right)$ represents a reduction factor by recomputing the actual evapotranspiration from crop potential evapotranspiration and actual soil moisture or relative soil moisture deficit.

Petrovic [25, 1984] showed that there is a large variability in the estimation of (4.6). Therefore, the relationship shown in Figure 4.2 was included in DAIR and is given by:

$$ET_{act} = \begin{array}{ll} ET_{crop} & \text{for } SM \geq SM_{crit} \\ ET_{crop}\frac{SM_{res}}{SM_{av}} & \text{for } SM_{wp} < SM < SM_{crit} \\ 0 & \text{for } SM \leq SM_{wp} \end{array} \tag{4.7}$$

$$SM_{res} = SM - SM_{wp} \tag{4.8}$$

with SM_{crit} within the range of the possible boundary between readily and not readily available soil moisture ($2.8 < pF < 2.0$) and SM_{res} is the total soil moisture above wilting pointing. The critical soil moisture SM_{crit} (in Fig. 4.2 shown as CRISMC) represents the value below which a next decrease of soil moisture will cause a decrease of ET_{act} and can change within the growing season and from plant to plant type. It is than the lower boundary of readily available soil moisture and is one of the parameters which can be used for fine tuning of the model. As a rule, SM_{crit} is equal to SM_{fc} in the first run of the model.

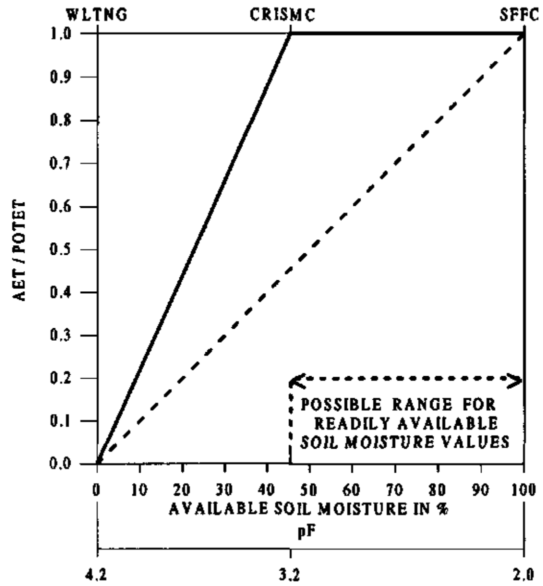

Figure 4.2: Relation between ratio of actual and potential evapotranspiration as a function of available soil moisture

4.2.5. Ground water level and runoff

The ground water level and runoff in DAIR are results of the simulated vertical hydrological balance. It is supposed that the runoff from the area Q_o exceeds the flow to the area Q_i, hence the calculated runoff represents just the contribution of the model areal unit to the runoff from the region.

Seepage contributes to the ground water reservoir, resulting in a ground water level rise whereas capillary rise uses water from this reservoir and causes a decrease of the ground water level h_{gw}. To evaluate changes of h_{gw} in the soil layer with given porosity equal to θ_s the penetration coefficient was introduced. In the present application the penetration coefficient C_{pen} [m mm^{-1}] represents the change of ground water level h_{gw} expressed in meters caused by an equivalent of 1 mm water layer of seepage or capillary rise (hysteresis is neglected). As a first approximation the C_{pen} can be described by:

$$C_{pen} = \frac{0.1}{\theta_s} \tag{4.9}$$

The initial or step by step computed ground water level is the base for runoff estimation. During the development of DAIR the application of three basic relations to compute runoff was proposed. Each of these functions may either be used separately or as a weighed contribution to simulated runoff. The most simple approach calculates runoff as a linear function of ground water level:

$$Q_o = a + b\, h_{gw} \tag{4.10}$$

in which a and b are tuning parameters which can be different for separate soil layers. The second approach is based on the bucket concept and is expressed by:

$$Q_o = c\, 10^{\frac{d}{h_{gw}}} \tag{4.11}$$

with c and d again tuning parameters which are constant over the entire ground water level range. The final approach is based on the antecedent precipitation index (API) concept. A modification was made to delimit the expected range of ground water levels by defining the relative ground water level $h_{gw\mathrm{ref}}$:

$$h_{gw\mathrm{ref}} = \frac{h_{gw} - h_{gw\,\mathrm{max}}}{h_{gw\,\mathrm{max}} - h_{gw\,\mathrm{min}}} \qquad h_{gw\,\mathrm{max}} \text{ deeper than } h_{gw\,\mathrm{min}} \tag{4.12}$$

The runoff is then computed according to:

$$Q_o = C_{API}\, API\, h_{gw\mathrm{ref}} \tag{4.13}$$

in which C_{API} is again a tuning coefficient.

The contribution of the model areal unit to the runoff is composed as a linear combination of the possible approaches (4.10), (4.11) and (4.13). The computed runoff causes a decrease of ground water level estimated in a manner like for seepage and capillary rise.

4.2.6. Additional options in DAIR

From a hydrological research point of view, it is worthful to mention that the DAIR model contains a snow routine, including snow pack accumulation, evaporation and melting processes. Furthermore, there is an option to simulate preferential flow through vertical soil cracks.

Evaluation of irrigation and the natural regime are performed completely parallel. There is a relatively large possibility to describe parameters for supplementary irrigation dosage and time scheduling. During a computation run it is assumed in the model that an irrigation dose is applied immediately when needed.

Processing of long term data series allows evaluation of trends of different variables like potential and actual evapotranspiration or needed amounts of supplementary irrigation. This aspect is very interesting when studying the impact of climatic change under continental conditions.

4.3. Model SWAP93

4.3.1. The basic flow equation

The flow of water in a heterogeneous soil-root system can be described by the one-dimensional Richards' equation extended by a sink term S for plant water uptake:

$$\frac{\partial \theta}{\partial t} = \frac{\partial}{\partial z}\left[k(\theta)\left(\frac{\partial h}{\partial z}+1\right) - S(h, ET_{pot})\right] \tag{4.14}$$

in which the vertical coordinate z [cm] is taken positive downward. The sink term S [cm d^{-1}] represents the water uptake by plant roots. The integral of the sink term over the rooting depth z_r yields the actual transpiration T_{act} or water uptake rate:

$$T_{act} = \int_{z=0}^{z=z_r} S \, \mathrm{d}z \tag{4.15}$$

Several authors have attempted to describe the function of S in terms of Ohm's law. In that case the water uptake rate is assumed to be directly proportional to the pressure head difference between the soil and the root interior, the soil hydraulic conductivity and a root "effectiveness" function [10, Feddes et al., 1974]. One of the major difficulties, however, remains the determination of this root effectiveness function. Therefore a more simplistic description was developed in which the water uptake is a direct function of pressure head, assuming that there is no difference between water uptake of the different roots over the entire root profile.

The general shape of the sink term S used in the model SWAP is shown in Figure 4.3. The assumptions made in the description of S are: under conditions wetter than the anaerobiosis point h_1 and conditions dryer than the wilting point h_4, water uptake by roots quickly reaches zero. The water uptake is maximal between the pressure head values h_2 and h_3 of which h_3 is the value below which roots cannot extract water optimally anymore. The position of h_3 depends upon the evaporative demand of the atmosphere, being h_{3H} for a high evaporative demand equal to 0.5 cm d^{-1} and h_{3L} for a low evaporative demand of 0.1 cm d^{-1}. The term α in Figure 4.3 is described according to:

$$\alpha(h) = \frac{S(h)}{S_{\max}} \tag{4.16}$$

Combining (4.15) and (4.16) yields:

$$T_{act} = \int_{z=0}^{z=z_r} \alpha(h) \, S_{\max} \, \mathrm{d}z \tag{4.17}$$

Under conditions of potential transpiration the root water uptake is maximal hence $\alpha = 1$, yielding:

$$T_{\text{pot}} = S_{\max} \int_{z=0}^{z=z_r} \mathrm{d}z \quad \Leftrightarrow \quad S_{\max} = \frac{T_{\text{pot}}}{z_r} \tag{4.18}$$

The Richards' equation (4.14) is a highly non-linear differential equation since $k(\theta)$ and $S(h(\theta), ET_{pot})$ depend upon the actual solution $\theta(z,t)$. Therefore, (4.14) can only be solved numerically for which the soil hydraulic properties $\theta(h)$ and $k(h)$, the initial conditions and boundary conditions at top and bottom of the soil system are needed.

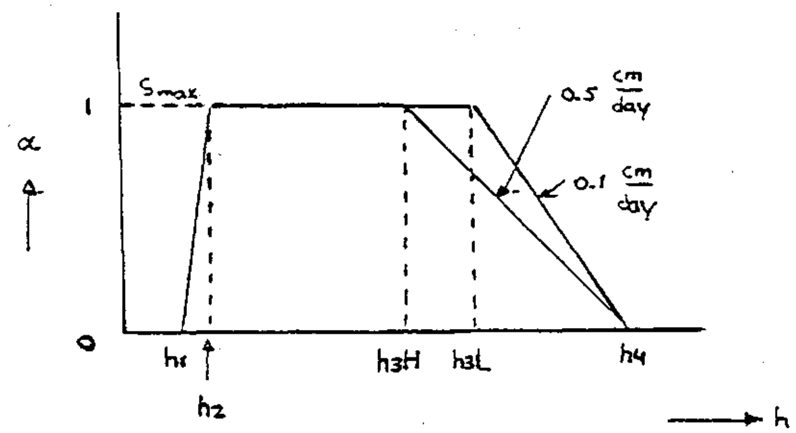

Figure 4.3: General shape of the sink term S as a function of pressure head and evaporative demand used in SWAP93 [Feddes et al., 1974]

4.3.2. Initial conditions and soil physical properties

In SWAP the hydraulic properties $\theta(h)$ and $k(h)$ are described analytically by the Van Genuchten equations (3.42) and (3.43). The hydraulic properties can be specified for different layers with a maximum of 5. The hysteresis option included in the model is not used in this study, hence only parameters for the drying or desorption curve are given $(a_{g\,\text{desorption}} = a_{g\,\text{adsorption}})$.

The initial conditions can be specified as either the volumetric soil moisture content θ or pressure head h at each nodal point. A third option is to start with pressure head values calculated by the model as being in equilibrium with the initial ground water level.

4.3.3. Bottom boundary conditions

Several options are available to describe the boundary conditions at the bottom of the modelled soil system. When the lower part of the soil column remains saturated during the entire calculation period the input can be given as a prescribed daily ground water level, a prescribed flux from the saturated zone or as a flux calculated by the model to a deep aquifer or the saturated zone. In case that the soil column remains unsaturated over the entire simulated depth during the calculation period, the bottom boundary can be described as a prescribed pressure head, a zero flux condition or free drainage.

4.3.4. Upper boundary conditions

At the upper boundary the model SWAP calculates the potential evapotranspiration ET_{pot} from daily values of meteorological input data like net radiation, air temperature, air humidity and wind velocity at 2 m height. Which input data are needed depends upon the chosen method: Priestley-Taylor, Penman, Monteith-Rijtema or Makkink (see 3.3). Furthermore, the input includes daily values of precipitation or, in case the clay module is used, 30 minute values of precipitation.

Based upon the potential evapotranspiration ET_{pot} and precipitation P the maximum possible flux through the canopy T_{pot} and through the surface q_s are determined. The following relationship was adopted to calculate T_{pot}:

$$T_{pot} = ET_{pot} - E_{pot} \tag{4.19}$$

in which E_{pot} is the potential soil evaporation.

Originally E_{pot} in the SWAP model can be calculated according to two methods. In the version used for this study, however, only the method described by Belmans et al. [1, 1983] was used:

$$E_{pot} = ET_{pot} \exp(-0.6LAI) \tag{4.20}$$

Once values of ET_{pot} and E_{pot} are known, T_{pot} is calculated according to (4.19) and used to determine the maximum possible root water uptake $S_{\max}$ in (4.18). The actual evapotranspiration ET_{act} is calculated as the sum of actual transpiration T_{act} given by (4.17) and actual evaporation E_{act}. The latter is obtained by applying either the reduction model of Black (3.45) or Boesten (3.46).

The maximum possible flux through the soil surface consists of two components:

$$q_s = E_{act} - (P - I) \tag{4.21}$$

in which I is the intercepted rainfall [$\mathrm{mm\,d^{-1}}$]. The flux q_s is positive in case of evaporation and negative during infiltration. The difference between rainfall and intercepted rainfall is that part of the rainfall that eventually reaches the soil surface (throughfall). In the used model version I was calculated according to (2.12).

4.3.5. Crack module

Recently a crack module was added to the SWAP model which can be used to describe changes in the vertical water movement due to swelling and shrinkage in clay soils. Swelling and shrinkage are supposed to follow a polygon pattern at the surface. Through the specified shrinkage characteristic SWAP calculates the crack depth and relative cross sectional area of the cracks at the soil surface. The matrix and crack infiltration is calculated separately according to [5, Bronswijk, 1991]:

$$\begin{array}{ll} P_i < I_{\max} & I_m = A_m P_i \\ & I_c = A_c P_i \\ P_i > I_{\max} & I_m = A_m I_{\max} \\ & I_c = A_m \left(P_i - I_{\max}\right) + A_c P_i \end{array} \tag{4.22}$$

in which P_i is rainfall intensity [$\mathrm{m\,s^{-1}}$], $I_{\max}$ maximum infiltration rate of soil matrix [$\mathrm{m\,s^{-1}}$], I_m and I_c infiltration into soil matrix and cracks respectively [$\mathrm{m\,s^{-1}}$] and A_m and A_c relative area of soil matrix respectively cracks [-].

As shown in Figure 4.4, water stored in the cracks W_c will either be absorbed by the soil matrix represented by the flux $q_{c,m}$ or flow rapidly to nearby drains or ditches represented by $q_{c,d}$. The absorption flux $q_{c,i}$ to soil compartment i can be described by:

$$q_{c,i} = -k\left(h_i\right)\frac{\partial H}{\partial x} = -k\left(h_i\right)\frac{h_i}{\frac{1}{4}D} \tag{4.23}$$

in which H is soil water potential [m] and x horizontal distance [m]. The total soil matrix flux $q_{c,m}$ is the sum of all compartment fluxes $q_{c,i}$ between the bottom of the crack and the water level in the crack. The bypass flow to drains or ditches $q_{c,d}$ is calculated similar to linear reservoirs:

$$q_{c,d} = k_d W_c \tag{4.24}$$

in which k_d is the rate coefficient for bypass flow to drains or ditches [$\mathrm{s^{-1}}$]. The change of water storage in the crack is finally calculated as:

$$\frac{\partial W_c}{\partial t} = I_c - q_{c,m} - q_{c,d} \tag{4.25}$$

Input data needed specifically for the crack module are rainfall intensity and the parameters e_o, ν_1 and ν_2 describing the shrinkage characteristic (3.44). Furthermore, the depth S_c at which the crack area A_c for surface infiltration is calculated, a geometry factor R_s and values of k_d and D are needed.

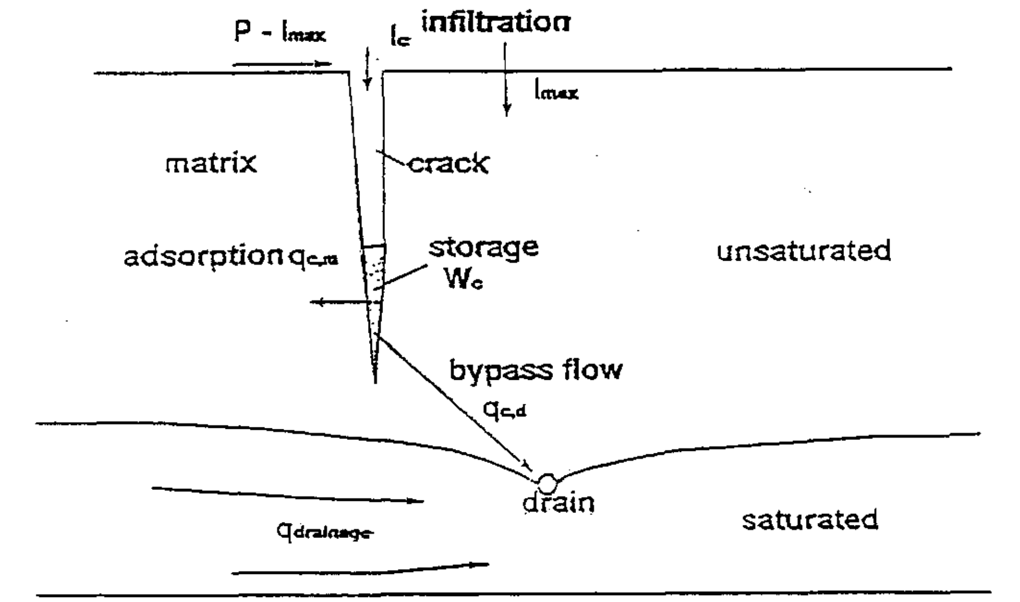

Figure 4.4: Schematic picture of water fluxes in a cracked soil [Bronswijk, 1988]

4.3.6. Additional changes

To validate SWAP93 using the data obtained in the Ziharec field experiment, some changes were made to the original model described in the instructions manual [38, Work group SWAP, 1994]. First, the model originally calculates the leaf area index LAI from soil cover whereas in the adjusted version LAI is also direct input. This LAI is used to calculate the potential evaporation according to (4.20).

Second, the original precipitation-interception function in SWAP was also based on soil cover. This function was replaced by equation (2.12) obtained for maize by Schmidt and Mueller [33, 1991].

5. Model validation

5.1. Results DAIR

The data collected during the field experiment were used to validate the model DAIR. Since model calculations must start at January 1, data collected at the meteorological station in Ziharec were used for the period prior to the start of the experiment. Only results for the period during which the field experiment was carried out are presented here.

For the start of the model simulations with DAIR at Jan 1 the initial conditions were optimized in order to obtain agreement with measured ground water level at the start of the field experiment (June 3). Additional input data were measured daily mean values of air temperature, air humidity and daily precipitation.

At the upper boundary the potential evapotranspiration was calculated according to Budyko's method multiplied by a crop factor according to (4.5). The crop factor k_c was taken as 1.05 during crop stage 3 and 0.6 during crop stage 4 (Table 5.1) according to Doorenbos and Pruitt [9, 1977]. Resulting ET_{pot} values of Budyko's method are compared to ET_{pot} calculated by the Priestley-Taylor method. For the latter, only data obtained directly from the field experiment are used. Figure 5.1 shows that Budyko's method yields a more uniform pattern with less extreme values than the Priestley-Taylor method. Obviously, this difference is caused by the limited values of ET_{pot} during a specific month as given in appendix C for Budyko's method, whereas the Priestley-Taylor method is based on daily measured meteorological data and hence has no specified upper or lower limits. The cumulative potential evapotranspiration over the field experimental period, however, is rather similar for both methods: 392 and 374 [mm] for Budyko's and Priestley-Taylor method respectively. To obtain the cumulative values, ET_{pot} was estimated from standard meteorological data when field data were missing.

The actual evapotranspiration is calculated from potential evapotranspiration and available soil moisture according to (4.6) and (4.7). The value of critical soil moisture SM_{crit} in (4.7) was chosen equal to SM_{fc} in the first computation run hence the dashed diagonal in Figure 4.2 represents the applied reduction. In case actual evapotranspiration calculated by a different method is available, the value of SM_{crit} could be used to tune and adjust model results. Within the

Table 5.1: Crop factors used in DAIR according to FAO standards [Doorenbos and Pruitt, 1977]

crop	stage	humidity	$RH_{\min} > 70\%$		$RH_{\min} < 20\%$	
		wind speed [m s^{-1}]	0-5	5-8	0-5	5-8
corn	3		1.05	1.1	1.15	1.2
	4		0.55	0.55	0.6	0.6

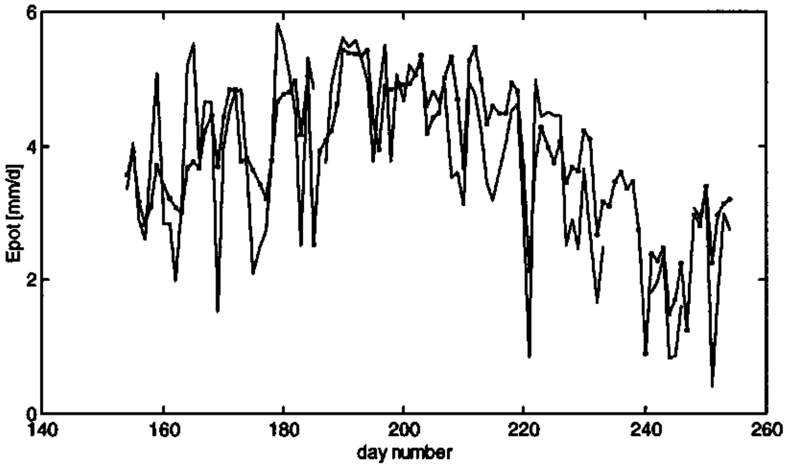

Figure 5.1: Potential evapotranspiration calculated by Budyko's method (**) and Priestley-Taylor method (—)

framework of this study, however, no results of additional methods were used. The value of SM_{av} is obtained after calculating the ground water level h_{gw} and runoff Q_o for which three methods are available given by (4.10), (4.11) and (4.13). Since it appeared that simulated ET_{act} in this study was hardly influenced by the chosen Q_o method (maximum daily difference 0.6 [mm], cumulative 7.6 [mm]), only results obtained when using (4.13) are presented here.

The resulting simulated values of ET_{act} and field results obtained by the standard flux profile method are shown in Figure 5.2. During periods for which field data are missing, ET_{act} was estimated from standard meteorological data. Figure 5.2a clearly shows that the deviation between simulated and measured values is rather large during the starting period and middle part of the field experiment, with simulated values being structurally lower respectively higher than field data. Possible causes of these deviations may be found in determination of ET_{pot} or reduction of ET_{pot} to ET_{act} based on available soil moisture. Since the differences in ET_{pot} from measured data (Priestley-Taylor method) and long-term climatic characteristics (Budyko's method) during these periods don't show similar large structural deviations (Fig. 5.1), the cause probably lies in the runoff or soil moisture routine.

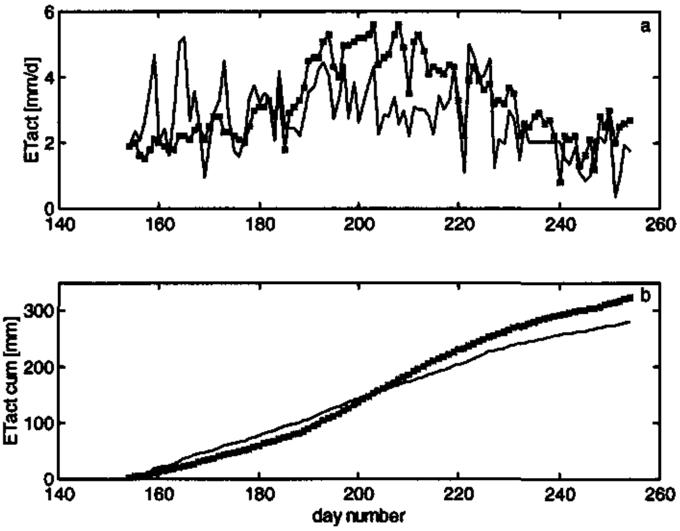

Figure 5.2: Simulated values of daily actual evapotranspiration (a) and cumulative values (b) (**) by DAIR compared to field data (-).

The ground water level h_{gw} is computed from calculated seepage Q_{seep} and capillary rise Q_{cap} as described in 4.2. The empirical coefficients $qflco1$ and $qflco2$ needed to calculate Q_{cap} by (4.1) were obtained from the soil water retention curve $\theta(h)$. The penetration coefficient C_{pen} describing the change of h_{gw} due to seepage or capillary rise was chosen as the reciprocal value of saturated moisture content θ_s. The resulting simulated and measured ground water level are shown in Figure 5.3. The general trend of decreasing h_{gw} during the field experiment is followed rather well during a drying period like in the middle part of the experiment. However, the sharp increase of h_{gw} to about 30 cm below soil surface in June as well as the changes after sequential wetting and drying in the last weeks of the experiment are not found in simulated values. The sharp increase to 30 cm was caused by continuing rainfall which could not be stored anymore in the nearly saturated soil profile. The incapability of DAIR to simulate such short term changes, indicates that the soil moisture routine is not functioning properly as found also for ET_{act} calculations (Fig. 5.2a).

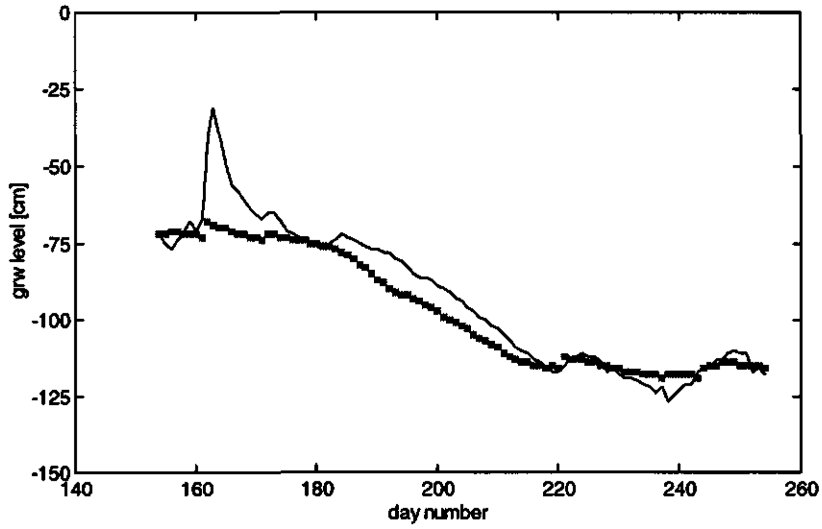

Figure 5.3: Ground water level simulated by DAIR (**) and field measured data (—)

5.2. Results SWAP93

The verification of the model SWAP93 was performed with the Priestley-Taylor method to calculate potential evapotranspiration at the upper boundary. At the bottom boundary, measured daily ground water level was given as input. The soil profile was taken as a one-layer system of 2 m depth with the hydraulic characteristics as presented in Table 3.1. As initial condition the measured soil moisture content at each nodal point was used (40 nodes) with intermediate values obtained by linear interpolation. Additional input data like leaf area index and rooting depth were all according to measured data. The resulting standard input file is given in Appendix D. In order to test the impact of the crack module described in 4.3.5, the results of two model simulation runs are described here being one run without and one including simulation of crack formation. When using the crack module, additional required input data are precipitation at 30 min intervals and parameters characterizing the shrinking characteristic (Table 3.3).

The potential evapotranspiration calculated by SWAP is 402 mm which is slightly higher than results presented in 3.5 (374 mm) since the soil heat flux G in

(3.36) is ignored. As mentioned in 3.3.4, the ET_{pot} resulting from the Priestley-Taylor method can be considered as a reference value which formally should be multiplied by a crop factor, this is however not standard practice and also not included in SWAP.

The model splits ET_{pot} into potential evaporation E_{pot} and transpiration T_{pot} according to (4.19). The result is shown in Fig. 5.4. For the reduction of E_{pot} the Boesten model (3.46) was used with coefficient $\beta = 0.63$ cm$^{0.5}$ and the potential transpiration T_{pot} is reduced according to (4.15). The resulting $ET_{act} = E_{act} + T_{act}$ is shown in Figure 5.5 for model runs with and without simulating soil crack formation. Obviously, the model run without implementing the crack module yields a reasonable simulation of measured actual evapotranspiration ET_{act} throughout the growing season with an average deviation between measured and simulated values of 0.6 mm. Relatively large differences are found on day 165 (2.8 mm) and in the period from day 234 to 240 during which however no field data are available and ET_{act} was estimated from standard meteorological data of the Ziharec station. The cumulative evapotranspiration over the growing season is simulated very well, yielding a total ET_{act} of 280 mm which is equal to the measured value.

Implementation of the crack module causes a sharp decrease of ET_{act} during the first part of the field experiment (Fig. 5.5a). This result is mainly caused by a strong decrease of evaporation compared to the former model run as shown in Figure 5.6. Since the calculation and reduction of E_{pot} is not influenced directly by crack formation, the effect of the crack module is obviously a smaller maximum Darcian flux at the surface which causes lower simulated values of E_{act}. During the dry-down period in July, the value of E_{act} becomes negligible and hence the difference between simulation runs with and without crack formation gets smaller.

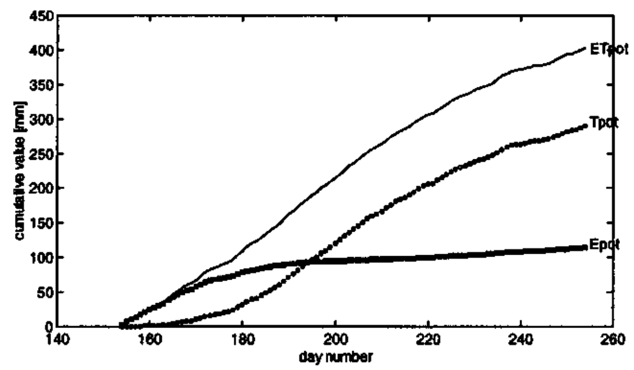

Figure 5.4: Potential evaporation E_{pot} and transpiration T_{pot} calculated by the model SWAP

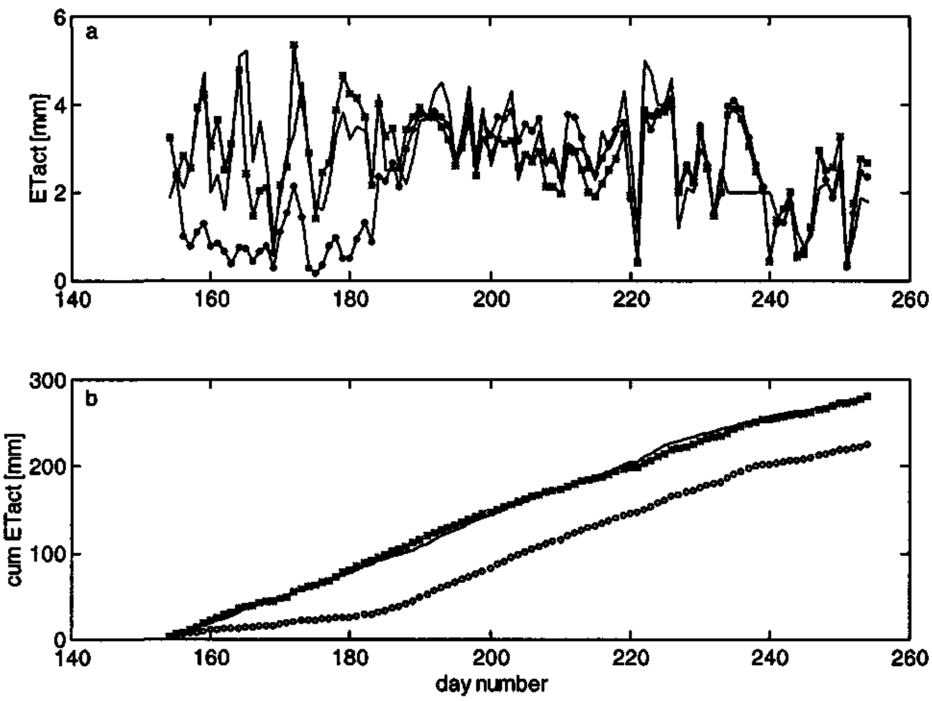

Figure 5.5: Daily values of actual evapotranspiration (a) and cumulative values (b) from field data (solid) and SWAP calculations (** no cracks, oo cracks simulated)

The model SWAP yields as output daily values of the volumetric soil moisture content θ and pressure head h at each nodal point. In order to compare simulated data with field measurements, three representative days were selected for which the measured and simulated data are shown in Figure 5.7. Only simulation without crack formation is shown since implementation of the crack module yielded similar results for the presented days. The selected days are: day 179 (June 28) immediately after a wet period with shallow ground water levels during the first period of the field experiment, day 219 (August 7) at the end of a long dry period in July with continuously decreasing ground water level and day 251 (September 8) towards the end of the field experiment. As can be seen in Fig. 5.7, there is a discrepancy between the saturated moisture content θ_s obtained from laboratory data (Table 3.1) and the 'field' θ_s resulting from the TDR calibration (Fig. 2.5) causing a structural difference between measured and simulated values. The general pattern of the vertical soil moisture profile, however, is followed rather well at day 179 and 219. At day 251 the measured profile is uniform with depth, while

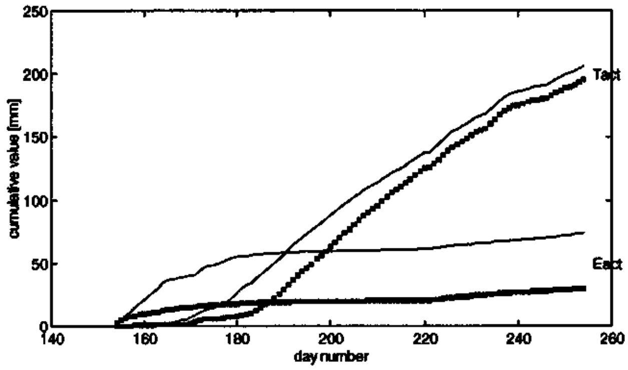

Figure 5.6: Cumulative actual transpiration and evaporation simulated without (solid) or with (**) implementation of the SWAP crack module

the simulated values show a clear water front at about 50 cm depth.

Based solely on these results, the implementation of the crack module offers no significant improvement in the water budget simulation. The sensitivity of the model to errors in the parameters characterizing the shrinking process, which were taken from literature values, was not tested however. Furthermore solute transport, being a factor significantly influenced by crack formation, was not considered in this study. A detailed sensitivity analysis of SWAP93, including the effect of using different ET_{pot} calculation methods and a multi-layer soil profile, was performed by Meijninger and Van Schaik [20, 1995]. Their analysis, however, did not include an extensive study of the crack module implementation.

5.3. Model comparison

The results of the models DAIR and SWAP93 can mainly be compared on the way the calculation and reduction of ET_{pot} is treated. Ground water level and soil moisture can not be compared since the ground water level is calculated by DAIR from seepage and capillary rise but given as input to the SWAP model. Similarly, soil moisture and hydraulic head profiles are given as output by SWAP whereas DAIR only uses a single total soil moisture value.

As described in 4, the main difference between the models lies in the conceptual base of DAIR with a simplified parameterization of the water movement in the soil profile and the physical base of SWAP solving the one-dimensional flow equation for small internal time-steps. Furthermore, the way potential evapotranspiration is determined is rather different.

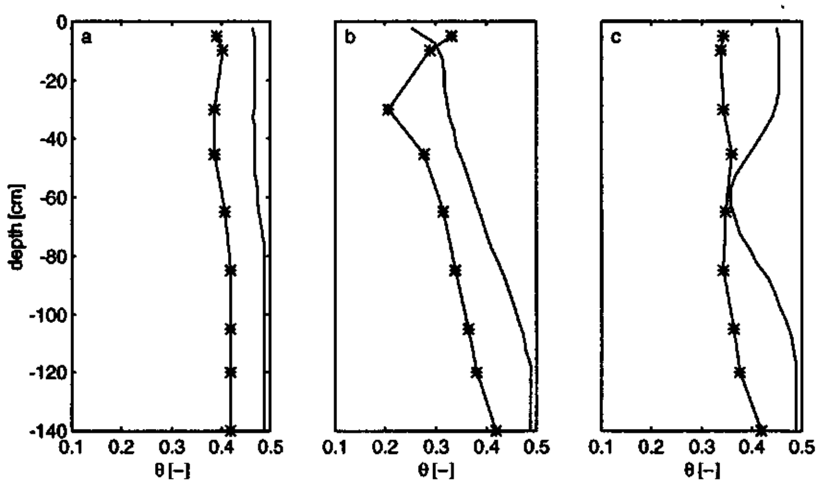

Figure 5.7: Measured (*) and simulated (solid line) vertical soil moisture profiles at day 179 (a), day 219 (b) and day 251 (c)

The cumulative potential evapotranspiration over the growing season is simulated rather adequate by both models. The reduction to ET_{act} is best performed by the model SWAP without including the crack module. Reduced evapotranspiration as resulting from DAIR is not very accurate which probable cause lies in the parameterization implied in the soil moisture and/or runoff routine as mentioned in 5.1. For the same reason, sudden changes in ground water level are not simulated well by DAIR. The general trend over the growing season, however, is again simulated rather adequate.

In general, the main points of further study for the SWAP model can be considered the effect of the clay module on evaporation calculations. A significant improvement to DAIR might be the implementation of a different routine for determining ET_{pot}, offering the possibility to simulate a wider range of meteorological conditions. An adjusted routine for determining the ground water level was already implemented in the model DINUND (see 4.1), implementing this routine standard in DAIR might improve the calculation of vertical soil water movement.

6. Conclusions and Recommendations

- **Field experiment**

The field data were used to calculate actual evapotranspiration by the standard flux profile method and Bowen ratio method. The results obtained by the Bowen ratio method appeared rather suspicious during several periods. However, no proper explanation for this problem was found. For future use, a similar installation of equipment and measurement set-up hence needs special attention with respect to the application of this method.

The comparison of actual evapotranspiration and soil moisture depletion on a short term base appears rather inaccurate. Over the entire field experiment, however, the different vertical water budget terms yield a nearly closed water balance.

Overall, a comprehensive set of meteorological data, hydrological data and crop parameters results from the field experiment. This data set can well be used for future model studies concerning the soil-water-plant-atmosphere system.

- **Potential evapotranspiration**

Several methods were applied to calculate potential evapotranspiration. Differences between the methods of Penman, Priestley-Taylor and Makkink are relatively small. When applying the methods of Monteith-Rijtema and Thom-Oliver the proper determination of resistance parameters, especially minimum bulk surface resistance, from available field data is questionable. Therefore, the Priestley-Taylor method is considered the most adequate for this study.

Budyko's method used in the model DAIR is based on long term meteorological data in typical climatic zones and hence not very suitable to determine daily potential evapotranspiration in a specific field situation.

- **Model results**

The potential evapotranspiration on a daily base is not simulated very accurately by the conceptual model DAIR, the cumulative value over the experimental period however is calculated quite well. The reduction to actual evapotranspiration shows large deviations compared to measured data. The average trend of changes in ground water level throughout the growing season is simulated properly but sudden changes in ground water level after rainfall are not calculated by DAIR. Major improvements might be achieved by incorporating a more physically based method to calculate potential evapotranspiration and an adjustment of the parameterization of the hydrological processes.

In the model SWAP the potential evapotranspiration was calculated by the Priestley-Taylor method which was also used to calculate ET_{pot} based upon field data. The validation run without using the recently added crack module yielded best results in simulations of actual evapotranspiration. Implementation of the crack module causes a too low evaporation during the first, relatively wet part of the field experiment. No serious effect was found on simulated soil moisture during model runs with or without crack formation. Additional research to study the impact of the crack module and model sensitivity to changes in shrinking characteristic parameters is recommended.

Generally spoken, results obtained by SWAP seem in better agreement with field data than simulated values by DAIR. However, the relatively small set of meteorological data and soil properties needed to run DAIR or any conceptual model in general may be an advantage when not much data are available for a specific situation. For use on a long term base, however, the effect of discrepancies between measured and simulated data should be tested thoroughly.

BIBLIOGRAPHY

[1] C. Belmans, J. Wesseling, and R. Feddes. Simulation model of the water balance of a cropped soil: SWATRE. *Water Resour. Res.*, 63:271–280, 1983.

[2] T. Black, W. Gardner, and G. Thurtell. The prediction of evaporation, drainage and soil water storage for a bare soil. *Soil Sci. Soc. Am. J.*, 33:655–660, 1969.

[3] C. Boast and T. Robertson. A "micro-lysimeter" method for determining evaporation from bare soil: description and laboratory evaluation. *Soil Sci. Soc. Am J.*, 46:689–696, 1982.

[4] J. Boesten and L. Stroosnijder. Simple model for daily evaporation from fallow tilled soil under spring conditions in a temperate climate. *Netherlands J. Agricult. Sci.*, 34:75–90, 1986.

[5] H. Bronswijk. *Magnitude, modeling and significance of swelling and shrinkage processes in clay soils.* PhD thesis, Department of Water Resources, Wageningen Agricultural University, 1991.

[6] W. Brutsaert. *Evaporation into the atmosphere; Theory, history and applications.* Kluwer Academic Publishers, Dordrecht, The Netherlands, 1982.

[7] J. De Boer. Warm water; warmte- en waterdampfluxen boven mais, Renkum 1985. Technical report, Department of Water Resources, Wageningen Agricultural University, 1988. MSc. thesis, In Dutch.

[8] H. De Bruin. *Micrometeorologie.* Department of Meteorology, Wageningen Agricultural University, 1995. In Dutch.

[9] J. Doorenbos and W. Pruitt. *Guidelines for predicting crop water requirements.* FAO Irrigation and drainage paper 24. FAO, Rome, 1977.

[10] R. Feddes, E. Bresler, and S. Neuman. Field test of a numerical model for water uptake by root systems. *Water Resour. Res.*, 10:1199–1206, 1974.

[11] R. Feddes, P. Kowalik, and H. Zaradny. *Simulation of field water use and crop yield.* Simulation Monograph. Pudoc, Wageningen, The Netherlands, 1978.

[12] E. Greacen. *Soil water assesment by the neutron method.* CSIRO, East Melbourne, Australia, 1981.

[13] A. Holtslag. Surface fluxes and boundary layer scaling. Technical Report 87-2, Royal Dutch Meteorological Institute, De Bilt, 1987.

[14] A. Jacobs, J. Halbertsma, and C. Przybyla. Behaviour of the crop resistance of maize during a growing season. estimation of areal evapotranspiration. *Proceedings of a workshop held at Vancouver, B.C., Canada, August 1987*, (177):165–173, 1989.

[15] D. Kim. *Characterization of swelling and shrinkage behaviour, hydraulic properties and modelling of water movement in a physically ripening marine clay soil.* PhD thesis, Catholic University Leuven, 1992.

[16] E. Klaghofer. Ein Beitrag zur Bestimmung der Verdunstung von einer freien Wasseroberfläche, von einem unbewachsenen und einem mit Gras bewachsenen Boden. Technical Report 22, Petzenkirchen, 1974.

[17] R. Koopmans, J. Stricker, and P. Petrovic. A comparison of six unsaturated zone models with data from the Hupselse Beek catchment, The Netherlands. proceedings of the international conference 'Hydrological research basins and the environment'. *TNO Comm. Hydrol. Res.*, (44), 1990.

[18] P. Koorevaar. *Fysische karakterisering van de bodem.* Department of Water Resources, Wageningen Agricultural University, 1995. In Dutch.

[19] P. Koorevaar, G. Menelik, and C. Dirksen. *Elements of soil physics.* Developments in Soil Science 13. Elsevier, 1983.

[20] W. Meijninger and A. Van Schaik. Water balance calculation and SWAP model results of a maize field experiment in Slovakia. Technical report, Department of Water Resources, Wageningen Agricultural University, 1995. MSc thesis.

[21] A. Monin and A. Obukhov. Basic laws of turbulent mixing in the ground layer of the atmosphere. *Tr. Geofiz. Instit. Akad. Nauk, S.S.S.R.*, 24:163–187, 1954.

[22] J. Monteith. Evaporation and environment. *Proc. Symp. Soc. Exp. Biol.*, 19:205–234, 1965.

[23] C. Paulson. The mathematical representation of wind speed and temperature profiles in the unstable atmospheric surface layer. *J. Appl. Meteor.*, 9:856–861, 1970.

[24] H. Penman. Natural evaporation from open water, bare soil and grass. *Proc. Roy. Soc. A. London*, (A193):120–145, 1948.

[25] P. Petrovic. Vertical hydrological balance and its one-dimensional simulation by the model "DAIR". Technical Report 65, Department of Hydraulics and Catchment hydrology, Wageningen Agricultural University, 1984.

[26] P. Petrovic. A mathematical model of evapotranspiration and irrigation requirement with respect to profile water balance. proceedings of a workshop on 'Estimation of areal evapotranspiration'. *IAHS Publ.*, (177), 1989.

[27] J. Philip. The theory of heat flux meters. *J. Geophys. Res.*, 66:571–579, 1961.

[28] C. Priestley and R. Taylor. On the assessment of the surface heat flux and evaporation using large scale parameters. *Monthly Weather Review*, 100:81–92, 1972.

[29] T. Reitsma. *Wind-profile measurements above a maize crop.* PhD thesis, Wageningen Agricultural University, 1978.

[30] P. Rijtema. *An analysis of actual evapotranspiration.* dissertatie lh-389, Landbouwhogeschool Wageningen, Wageningen, The Netherlands, 1965.

[31] K. Roth, R. Schulin, H. Fluhler, and W. Attinger. Calibration of time domain reflectometry for water content measurement using a composite dielectric approach. *Water Resour. Res.*, 26:2267–2273, 1990.

[32] Russian State Hydrological Institute. *Recommendation for evapotranspiration estimation from the land surface.* Gidrometeoizdat, Leningrad, Russia, 1976. In Russian.

[33] K. Schmidt and K. Mueller. Ergebnisse zur Niederschlags-Interzeption in landwirtschaftlichen Pflanzenbestaenden. *Z. Pflanzenernaehr. Bodenk.*, 154:153–156, 1991.

[34] G. Szeicz and I. Long. Surface resistance of crop canopies. *Water Resour. Res.*, 5:622–633, 1969.

[35] A. Thom and H. Oliver. On Penman's equation for estimating regional evaporation. *Quart. J. Roy. Meteorol. Soc.*, 103:345–357, 1977.

[36] TNO. Van Penman naar Makkink, een nieuwe berekeningswijze voor de klimatologische verdampingsgetallen. Technical Report 19, Commissie voor hydrologisch onderzoek TNO, 1988. In Dutch.

[37] M. Van Genuchten. A closed-form equation for predicting the hydraulic conductivity of unsaturated soils. *Soil Sci. Soc. Am. J.*, 44:892–898, 1980.

[38] Work Group SWAP. SWAP 1993; input instructions manual. Technical Report 45, Department of Water Resources, Wageningen Agricultural University, 1994.

[39] J. Wösten, G. Veerman, and J. Stolte. Waterretentie- en doorlatendheidskarakteristieken van boven- en ondergronden in Nederland: de Staringreeks. Technical Report 18, DLO-Staring Centrum, Wageningen, 1994. In Dutch.

A. Daily values of radiation, soil heat flux and actual evapotranspiration

Daily values (24 h) of the fluxes measured during the field experiment after necessary corrections. Presented fluxes are soil heat flux at the surface G, net radiation, incoming short-wave radiation $R_{s\downarrow}$, reflected short-wave radiation $R_{s\uparrow}$, sensible heat flux H and latent heat flux L_vE. All fluxes are given in [$\mathrm{W\,m^{-2}}$]. Values of H and L_vE are calculated by either the standard flux profile method or Bowen ratio method (at sunset/sunrise Bowen ratio fluxes replaced by flux profile results).

Missing data are indicated by (a): missing data due to a instrument or data-logger failure or (b): no wet bulb temperature profile measured.

						flux profile		Bowen ratio	
day nr	date	G	R_n	$R_{s\downarrow}$	$R_{s\uparrow}$	H	L_vE	H	L_vE
154	30695	-4	121	204	17	70	55	92	34
155	40695	14	158	265	24	76	67	98	45
156	50695	-2	99	149	11	43	59	41	61
157	60695	0	91	139	10	16	75	24	68
158	70695	7	139	199	13	28	105	32	101
159	80695	16	186	284	19	37	134	74	97
160	90695	9	104	163	13	37	58	34	61
161	100695	31	130	184	13	30	69	28	71
162	110695	25	93	145	12	22	46	10	58
163	120695	17	126	181	15	28	81	23	86
164	130695	14	193	268	22	35	144	44	135
165	140695	10	200	281	24	42	149	56	135
166	150695	-1	135	223	23	59	76	84	51
167	160695	19	180	302	33	59	102	74	88
168	170695	18	176	309	35	84	74	101	57
169	180695	-1	53	117	14	26	27	61	-8
170	190695	28	160	275	33	78	55	107	26

						flux profile		Bowen ratio	
day nr	date	G	R_n	$R_{s\downarrow}$	$R_{s\uparrow}$	H	L_vE	H	L_vE
171	200695	32	178	315	38	64	83	85	62
172	210695	25	175	284	34	56	94	76	75
173	220695	-22	143	214	19	37	128	37	128
174	230695	-5	128	223	24	55	78	44	90
175	240695	2	78	128	14	27	49	22	54
176	250695	2	89	142	16	42	45	35	52
177	260695	3	97	147	16	31	63	30	64
178	270695	10	136	195	20	31	95	30	95
179	280695	16	208	325	39	85	107	70	123
180	290695	15	200	338	44	92	92	57	128
181	300695	25	188	323	48	63	100	36	126
182	10795	26	167	310	40	45	96	15	126
183	20795	4	83	170	24	21	59	12	68
184	30795	23	186	295	40	44	119	44	120
185	40795	5	161	263	37	87	70	b	b
186	50795	a	a	a	a	a	a	b	b
187	60795	10	135	249	36	55	70	b	b
188	70795	17	177	311	46	97	63	b	b
189	80795	19	187	316	46	88	80	b	b
190	90795	22	195	314	46	72	101	43	130
191	100795	17	185	308	47	62	106	44	123
192	110795	17	188	309	47	50	121	58	113
193	120795	18	179	283	44	34	127	42	119
194	130795	16	165	262	42	34	115	40	110
195	140795	7	124	194	30	39	78	35	82
196	150795	4	154	234	37	54	97	48	102
197	160795	14	183	291	46	44	125	75	95
198	170795	7	126	222	36	42	78	43	77
199	180795	14	175	285	47	50	110	42	119
200	190795	13	159	262	43	71	75	50	98
201	200795	16	180	305	51	72	92	44	120
202	210795	18	175	298	50	49	109	74	83
203	220795	17	176	292	51	36	123	-9	202
204	230795	6	153	251	45	83	64	53	94
205	240795	14	171	296	52	76	81	68	92

						flux profile		Bowen ratio	
day nr	date	G	R_n	$R_{s\downarrow}$	$R_{s\uparrow}$	H	L_vE	H	L_vE
206	250795	12	164	293	53	72	80	57	95
207	260795	17	172	295	53	59	97	38	118
208	270795	13	122	247	47	35	73	6	103
209	280795	10	124	197	37	28	85	24	90
210	290795	6	106	186	37	36	63	27	73
211	300795	15	168	292	56	65	88	61	92
212	310795	15	162	287	54	60	86	53	94
213	10895	11	144	262	50	48	86	12	123
214	20895	4	117	225	45	33	80	25	88
215	30895	7	111	211	43	39	64	63	70
216	40895	7	126	223	44	21	98	40	79
217	50895	12	142	249	49	44	86	58	72
218	60895	10	155	290	57	50	95	24	121
219	70895	15	161	261	51	23	123	15	129
220	80895	-4	91	151	30	13	82	21	74
221	90895	-9	20	48	10	-1	31	2	28
222	100895	3	168	276	54	22	143	b	b
223	110895	0	145	273	54	12	133	b	b
224	120895	-2	149	282	56	35	115	b	b
225	130895	2	149	268	53	32	115	b	b
226	140895	7	150	268	53	14	130	b	b
227	150895	-6	78	175	37	49	35	38	46
228	160895	2	101	192	39	40	60	44	55
229	170895	2	84	161	33	26	56	22	60
230	180895	7	124	220	45	31	85	28	88
231	190895	5	92	168	33	9	77	9	77
232	200895	0	54	104	21	13	42	16	39
233	210895	-9	73	131	26	10	72	16	66
234	220895	a	a	a	a	a	a	a	a
235	230895	a	a	a	a	a	a	a	a
236	240895	a	a	a	a	a	a	a	a
237	250895	a	a	a	a	a	a	a	a
238	260895	a	a	a	a	a	a	a	a
239	270895	a	a	a	a	a	a	a	a
240	280895	a	a	a	a	a	a	a	a

						flux profile		Bowen ratio	
day nr	date	G	R_n	$R_{s\downarrow}$	$R_{s\uparrow}$	H	L_vE	H	L_vE
241	290895	-7	63	132	25	27	43	29	42
242	300895	-7	71	154	30	39	38	26	51
243	310895	-4	88	164	31	39	53	45	48
244	10995	-7	26	53	10	2	31	6	27
245	20995	-2	32	67	12	9	24	7	27
246	30995	1	61	110	20	31	28	29	31
247	40995	a	a	a	a	a	a	a	a
248	50995	9	123	231	43	53	62	31	83
249	60995	7	113	207	38	49	57	29	77
250	70995	10	127	220	42	39	78	12	115
251	80995	1	15	58	11	4	10	-12	28
252	90995	4	66	142	26	36	27	12	51
253	100995	1	109	217	41	52	55	53	55
254	110995	7	102	172	32	45	50	39	54

B. Daily potential evapotranspiration by different methods

Daily values of potential evapotranspiration [mm] calculated by the methods described in 3.3. Missing data due to an instrument or datalogger failure are indicated by (a). Additionally daily results of Budyko's method used in the model DAIR (see 5.2) are given.

day nr	date	Priestley-Taylor	Penman	Makkink	Budyko
154	30695	3.4	4.1	2.8	3.6
155	40695	4.1	4.1	3.9	3.9
156	50695	2.9	2.9	2.2	3.2
157	60695	2.6	2.5	2.0	2.8
158	70695	3.8	3.5	2.9	3.1
159	80695	5.1	4.6	4.4	3.7
160	90695	2.8	2.9	2.5	3.4
161	100695	2.9	2.8	2.7	3.2
162	110695	2.0	2.1	2.2	3.1
163	120695	3.1	2.9	2.7	3.0
164	130695	5.2	4.9	4.0	3.7
165	140695	5.5	5.1	4.2	3.8
166	150695	3.8	3.7	3.3	3.7
167	160695	4.7	4.6	4.5	4.2
168	170695	4.6	4.8	4.7	4.5
169	180695	1.5	1.8	1.7	3.7
170	190695	4.0	4.2	4.3	4.4
171	200695	4.5	4.5	5.0	4.8
172	210695	4.8	5.0	4.7	4.8
173	220695	4.8	5.1	3.2	3.8
174	230695	3.6	3.9	3.1	3.8
175	240695	2.1	2.3	1.8	3.7

day nr	date	Priestley-Taylor	Penman	Makkink	Budyko
176	250695	2.5	2.9	2.1	3.4
177	260695	2.7	3.0	2.2	3.2
178	270695	3.8	4.2	3.1	3.8
179	280695	5.8	6.9	5.1	4.7
180	290695	5.5	6.2	5.2	4.8
181	300695	5.1	5.1	5.2	4.8
182	10795	4.5	4.5	5.1	5.0
183	20795	2.5	2.9	2.8	4.2
184	30795	5.3	5.9	5.0	5.1
185	40795	4.9	4.1	4.2	2.5
186	50795	a	a	a	3.9
187	60795	3.7	3.0	3.8	4.1
188	70795	4.9	3.9	4.9	4.2
189	80795	5.3	5.1	5.2	4.6
190	90795	5.6	5.7	5.3	5.4
191	100795	5.5	5.9	5.2	5.4
192	110795	5.6	5.6	5.2	5.4
193	120795	5.3	5.2	4.8	5.4
194	130795	5.0	5.5	4.5	5.4
195	140795	3.8	3.8	3.2	4.4
196	150795	4.8	4.6	3.8	3.9
197	160795	5.5	5.8	4.9	4.9
198	170795	3.8	4.4	3.6	4.8
199	180795	5.1	5.4	4.7	4.9
200	190795	4.7	5.7	4.3	4.9
201	200795	5.2	5.6	5.0	4.9
202	210795	5.1	5.3	5.0	5.1
203	220795	5.3	5.8	5.0	5.4
204	230795	4.6	5.3	4.0	4.2
205	240795	4.8	5.6	4.7	4.4
206	250795	4.7	4.7	4.6	4.5
207	260795	4.9	5.1	4.8	5.0
208	270795	3.5	4.6	4.1	5.3
209	280795	3.6	4.2	3.2	4.7
210	290795	3.1	3.1	3.0	3.8

day nr	date	Priestley-Taylor	Penman	Makkink	Budyko
211	300795	4.9	5.7	4.9	5.3
212	310795	4.8	5.1	4.8	5.5
213	10895	4.3	4.8	4.3	5.0
214	20895	3.4	4.0	3.5	4.3
215	30895	3.2	4.2	3.4	4.6
216	40895	3.6	4.1	3.5	4.5
217	50895	4.0	4.7	4.0	4.5
218	60895	4.5	5.0	4.7	4.9
219	70895	4.6	4.9	4.3	4.8
220	80895	3.0	3.2	2.4	3.7
221	90895	0.9	0.9	0.7	2.2
222	100895	5.0	4.1	4.3	3.8
223	110895	4.4	3.5	4.3	4.3
224	120895	4.5	3.6	4.4	4.0
225	130895	4.5	3.5	4.2	3.8
226	140895	4.5	4.2	4.3	4.1
227	150895	2.5	3.4	2.7	3.4
228	160895	2.9	3.7	2.9	3.8
229	170895	2.5	2.7	2.5	3.6
230	180895	3.7	4.1	3.6	4.2
231	190895	2.7	3.1	2.7	4.1
232	200895	1.7	1.7	1.7	2.7
233	210895	2.5	2.6	2.1	3.2
234	220895	a	a	a	3.1
235	230895	a	a	a	3.5
236	240895	a	a	a	3.6
237	250895	a	a	a	3.4
238	260895	a	a	a	3.5
239	270895	a	a	a	2.7
240	280895	a	a	a	0.9
241	290895	1.8	2.5	1.8	2.4
242	300895	2.0	2.4	2.0	2.3
243	310895	2.4	2.8	2.2	2.5
244	10995	0.8	1.0	0.7	1.5
245	20995	0.9	1.1	0.9	1.7

day nr	date	Priestley-Taylor	Penman	Makkink	Budyko
246	30995	1.6	1.8	1.6	2.3
247	40995	a	a	a	1.3
248	50995	3.1	3.4	3.2	3.0
249	60995	2.9	2.9	2.9	2.8
250	70995	3.4	4.1	3.3	3.4
251	80995	0.4	0.8	0.9	2.3
252	90995	1.8	2.6	2.1	3.0
253	100995	3.0	3.3	3.1	3.1
254	110995	2.7	3.4	2.6	3.2

C. DAIR POTENTIAL EVAPOTRANSPIRATION

Daily potential evapotranspiration [$\mathrm{mm\,d^{-1}}$] as a function of vapour pressure deficit VPD [mbar] in tabular form as used by the DAIR model

	month										
VPD	I/XII	II	III	IV	V	VI	VII	VIII	IX	X	XI
0	0.08	0.10	0.16	0.25	0.57	1.33	0.97	0.39	0.23	0.13	0.10
1	0.40	0.55	0.74	1.17	1.71	2.43	2.13	1.39	0.93	0.65	0.57
2	0.71	0.92	1.29	1.82	2.36	2.90	2.63	2.07	1.55	1.27	0.95
3	0.97	1.27	1.73	2.27	2.77	3.27	3.00	2.50	2.02	1.52	1.28
4	1.10	1.58	2.09	2.65	3.07	3.59	3.23	2.84	2.40	1.84	1.63
5	1.44	1.86	2.40	3.00	3.37	3.88	3.61	3.14	2.75	2.16	1.92
6		2.08	2.68	3.27	3.61	4.13	3.86	3.40	3.06	2.40	2.15
7		2.29	2.96	3.57	3.86	4.37	4.10	3.64	3.33	2.68	2.37
8				3.80	4.08	4.60	4.31	3.87	3.58		
9				4.03	4.29	4.82	4.52	4.10	3.82		
10				4.23	4.47	5.00	4.71	4.29	4.02		
11					4.66	5.18	4.89	4.45			
12					4.82	5.35	5.05	4.63			
13					4.98	5.52	5.23	4.81			
14					5.15	5.68	5.37	4.95			
15					5.29	5.83	5.50	5.10			
16					5.44	5.95	5.63	5.24			
17					5.58	6.08	5.76	5.39			
18					5.71	6.20	5.89	5.52			

D. STANDARD INPUT FILE OF THE MODEL SWAP

GENERAL

```
>genhdr: 'Mais on heavy clay; analysis of growing season'
>output: 0 1 'outputseason.bal'
>exfile: 1 'soilprofile.prf' 1 1 0 0 0 0
>timeva: 1995 1995 154 254 1.0e-6 0.2 2 1.0e-3
>crack: 0
>redeva: 2 0.63
>irriva: 0
>methdr: 'meteorological conditions in growing season'
>topbnd: 2 1
>metfil: 1995 'meteo.dat'
>crphdr: 'maize Slovakya 1995'
>sinkva: 0 0 0
>rootac: 0. 365. 366.
>excons: 1.26
>crpfil: 1995 'swap93.inp'
>crppro: 0
>profil: 2 40 20 40 5 5 5 5 5 5 5 5 5 5 5 5 5 5 5 5 5 5 5 5 5 5 5 5 5 5 5 5 5 5 5 5
5 5 5 5 5 5 5 5
>soilfl: 'swap93.inp' 'swap93.inp'
>pondmx: 0.0
>incond: 0 0.424 0.429 0.413 0.397 0.380 0.364 0.369 0.374 0.379 0.376 0.372 0.369
0.366 0.363 0.489 0.489 0.489 0.489 0.489 0.489 0.489 0.489 0.489 0.489 0.489 0.489
0.489 0.489 0.489 0.489 0.489 0.489 0.489 0.489 0.489 0.489 0.489 0.489 0.489 0.489
>bbdfil: 'swap93.inp'
>drains: 0
>solute: 0
```

>mobile: 0

>anafil: 0

>balance: 0

CROP PARAMETERS————————————————

>sink95: -15. -30. -30. -325. -600. 999. -8000.

>root95: 1 154 10. 173 50. 202 110. 254 110.

>lasc95: 0.0280 2.9100 0.9570

>prin95: 0

>soco95: 1 154 0.034 156 0.036 164 0.270 175 1.060 188 2.720 199 5.290 222 3.990 242 2.84 255 2.757

SOIL PHYSICAL CHARACTERISTICS————————————————

>solhdl: 'Topsoil of heavy clay'

>metho1: 1

>soild1: 0 0.489 15.46 0.0532 -8.823 1.081 0

>solhd2: 'Subsoil of sandy clay'

>metho2: 1

>soild2: 0 0.489 15.46 0.0532 -8.823 1.081 0

BOTTOM BOUNDARY————————————————

>bothdr: 'Groundwater boundary'

>swbotb: 0

>daygwl: 11 154 -72 155 -75 156 -77 157 -74 158 -71 159 -68 160 -71 161 -67 162 -42 163 -31 164 -40 165 -49 166 -56 167 -58 168 -61 169 -64 170 -66 171 -67 172 -65 173 -65 174 -68 175 -71 176 -72 177 -73 178 -74 179 -75 180 -76 181 -77 182 -75 183 -74 184 -72 185 -73 186 -74 187 -75 188 -76 189 -77 190 -77 191 -78 192 -78 193 -80 194 -81 195 -83 196 -85 197 -86 198 -86 199 -87 200 -89 201 -90 202 -91 203 -93 204 -94 205 -96 206 -97 207 -99 208 -100 209 -102 210 -103 211 -105 212 -107 213-109 214 -110 215 -111 216 -113 217 -114 218 -116 219 -117 220 -117 221 -115 222 -113 223 -112 224 -111 225 -112 226 -112 227 -114 228 -117 229 -116 230 -118 231 -119 232 -119 233 -120 234 -121 235 -122 236 -124 237 -122 238 -127 239 -125 240 -123 241 -121 242 -121 243 -117 244 -116 245 -116 246 -113 247 -113 248 -111 249 -110 250 -111 251 -111 252 -117 253 -116 254 -118